

# The FLUKA atmospheric neutrino flux calculation

G. Battistoni<sup>a</sup>, A. Ferrari<sup>b</sup>, T. Montaruli<sup>c</sup>, P.R. Sala<sup>d</sup>

<sup>a</sup>INFN and Università di Milano, Dipartimento di Fisica, Milano, 20133, Italy

<sup>b</sup>CERN, Geneva 23, Switzerland, on leave of absence from INFN, Milano.

<sup>c</sup>Dipartimento di Fisica dell'Università e INFN, Bari

<sup>d</sup>ETH, Zurich, Switzerland, on leave of absence from INFN, Milano.

The 3-dimensional (3-D) calculation of the atmospheric neutrino flux by means of the FLUKA Monte Carlo model is here described in all details, starting from the latest data on primary cosmic ray spectra. The importance of a 3-D calculation and of its consequences have been already debated in a previous paper. Here instead the focus is on the absolute flux. We stress the relevant aspects of the hadronic interaction model of FLUKA in the atmospheric neutrino flux calculation. This model is constructed and maintained so to provide a high degree of accuracy in the description of particle production. The accuracy achieved in the comparison with data from accelerators and cross checked with data on particle production in atmosphere certifies the reliability of shower calculation in atmosphere.

The results presented here can be already used for analysis by current experiments on atmospheric neutrinos. However they represent an intermediate step towards a final release, since this calculation does not yet include the bending of charged particles in atmosphere. On the other hand this last aspect, while requiring a considerable effort in a fully 3-D description of the Earth, if a high level of accuracy has to be maintained, does not affect in a significant way the analysis of atmospheric neutrino events.

## 1. Introduction

Reliable calculations of flux of secondary particles in atmosphere, produced by the interactions of primary cosmic rays, are essential for the correct interpretation of the large amount of experimental data produced by experiments in the field of astroparticle physics. The increasing accuracy of modern experiments demands also an improved quality of the calculation tools. The most important example in this field is the analysis of the experimental results on atmospheric neutrinos from Super-Kamiokande[ 1], MACRO[ 2] and Soudan2[ 3], which gave the first robust evidence in favor of neutrino oscillations. The interpretation in terms of the mixing parameters is affected by different sources of systematic errors, and the theoretical uncertainties on neutrino fluxes and cross sections constitute a significant fraction of them. This has stimulated different efforts to improve the existing flux calculations. Among them, one is the calculation based on the FLUKA

Monte Carlo code[ 4]. Such a work was indeed started before[ 5] the Super-Kamiokande results, in the framework of design work for the ICARUS experiment[ 6] and of the analysis of MACRO experiment at Gran Sasso. The main motivation to propose the FLUKA based calculation was the idea that, in order to accomplish the goals summarized before, the highest degree of detail and accuracy should be accomplished.

In particular the FLUKA code is known for the accuracy of its particle production model in hadronic interactions, which is extensively benchmarked against accelerator data. The first important achievement obtained using FLUKA concerned the relevance of 3-D geometry in the flux calculations and was presented in ref.[ 7]. However, at the time of that work it was not yet possible to make statements on the absolute values of neutrino fluxes. This is instead the purpose of the present paper, which is intended to provide a complete reference for the FLUKA neutrino flux.

In the following, we shall first summarize the main ingredients of the simulation, discussing with some detail the primary cosmic ray spectrum and the geometrical set-up. Then, in a next section, we shall discuss the physics models of FLUKA presenting a set of comparisons between data and predictions to demonstrate the validity of the models themselves. The final results on the flux are presented and discussed, also by means of a comparison to other calculation results. Neutrino fluxes are calculated for 3 relevant experimental sites (Kamiokande, Gran Sasso and Soudan) and representative tables are given here for the Kamiokande site. More detailed tables for all the 3 sites are available on the web[ 8]. The energy region considered in this work ( $0.1 \div 200$  GeV) covers in practice the production of the event topologies of sub-GeV and multi-GeV events as detected in Super-Kamiokande.

In the conclusions we shall debate the level of systematic error in the predictions and mention the items that will require further improvements.

## 2. The Simulation Set-up

The flux calculation has been completely carried out in the framework of the FLUKA Monte Carlo code[ 4]. This is an interaction and transport MonteCarlo package able to treat with a high degree of detail the following problems:

- Hadron-hadron and hadron-nucleus interactions (0-100 TeV);
- Electromagnetic and  $\mu$  interactions (1 keV-100 TeV);
- Charged particle transport - ionization energy loss;
- Low energy neutron multigroup transport and interactions (0-20 MeV)

In the following we present some detail about the essential elements of the calculation, *i.e.* the geometrical description of the problem , the primary spectrum, the geomagnetic model and the treatment of solar modulation.

### 2.1. Simulation geometry, description of Earth and of its atmosphere

In view of applications for cosmic ray physics, we have implemented a 3-D spherical representation of the whole Earth and of the surrounding atmosphere. The radius of the

Earth sphere is assumed to be  $R = 6378.14$  km. The atmosphere is described by a medium composed by a proper mixture of N, O and Ar, arranged in 100 concentric spherical shells, each one having a density scaling according to the known profile of “standard atmosphere” [ 9] (see Fig. 1). This can be considered an improvement with respect to the work of ref.[ 7], where only 51 shells were considered. However, we could not find any significant changes in all test runs that we performed comparing results for the two different realizations of the atmosphere.

It should be noticed that, as in the other standard neutrino calculations, we are using the same description of the atmosphere profile over the whole Earth, while it is known that there exist differences as a function of latitude[ 10] and as a function of time during the year. This in principle is a source of systematic error, that will be discussed in section 7.

## 2.2. The Primary C.R. spectrum

In the first reference of FLUKA neutrino flux, the original Bartol spectrum of all nucleon flux was used[ 11]. The calculation presented here makes use of the fit of the recent cosmic ray measurements presented in [ 12] to recent cosmic ray flux measurements. In addition, the authors of [ 12] take into account the statistical errors of measurements and the systematic differences between different experiments in order to establish a band of uncertainty around the average result of this new fit.

The functional form adopted by Bartol to fit the data point as a function of the kinetic energy per nucleon ( $E_k$ ) is:

$$\phi(E_k) = K \times \left( E_k + b \exp \left[ -c\sqrt{E_k} \right] \right)^{-\gamma} \quad (1)$$

In Table 1 we report the values of the four fit parameters ( $K$ ,  $b$ ,  $c$  and  $\gamma$ ) for the different mass groups considered by Bartol. The higher and lower extremes for the proton components are obtained by considering only the error on  $K$ . The central value for the nuclear components is obtained by the average of the “High” and “Low” parameter values.

Table 1

Fit parameters from Ref. [ 12] for the main five components of the primary cosmic rays

component/fit	$< A >$	$\gamma$	$K$ $cm^{-2} s^{-1} sr^1 (GeV/A)^{-1}$	$b$ $GeV/A$	$c$ $(GeV/A)^{-0.5}$
protons	1	$2.74 \pm 0.01$	$14900 \pm 600$	2.15	0.21
He (high)	4	$2.64 \pm 0.01$	$600 \pm 30$	1.25	0.14
He (low)	4	$2.74 \pm 0.03$	$750 \pm 100$	1.50	0.30
CNO (high)	14	2.70	68	1.78	0.02
CNO (low)	14	” ”	55	” ”	” ”
MgSi (high)	26	” ”	22	” ”	” ”
MgSi (low)	26	” ”	18	” ”	” ”
$z > 17$ (high)	50	” ”	5.50	” ”	” ”
$z > 17$ (low))	50	” ”	5.20	” ”	” ”

Primary particles, sampled from such continuous spectra, are injected at the top of the atmosphere, at about 100 km of altitude. The primary flux is assumed to be uniform and isotropic. In case of primary nuclei, individual nucleons are unpacked before interaction, according to the the superposition model, since the present version of FLUKA code does not yet handle nuclear projectiles (see section 3).

The flux of all possible secondary products are scored at different heights in the atmosphere and at the earth boundary. Therefore, we are able to get, besides neutrino fluxes, the flux of muons and hadrons to be used for the benchmarking against existing experimental data.

### 2.3. The Geomagnetic Field

For our calculation we have adopted the IGRF model for geomagnetic field, which is expressed as an expansion of spherical harmonics[ 13]. A complete calculation within the 3-D Earth geometry should include geomagnetic effects both to introduce primary cutoff and to include charged particle bending during shower development[ 14]. The cutoff must be explicitly computed for each cosmic ray taken into consideration. In principle, one should consider primary cosmic rays from all directions over the whole Earth surface, and then, after applying the cutoff, count the neutrino reaching an area around the location of interest sufficiently small to avoid any significant change in the geomagnetic cutoff (*i.e.* few square degrees or less). This procedure does not allow to exploit the spherical symmetry to minimize computer power, since a realistic description of the magnetic field makes each point different from the other. However, the solutions so far adopted in ref. [ 14] and [ 19] are still unsatisfactory. In ref.[ 19] the authors make use of a dipole field both for geomagnetic cutoff test and particle simulation in atmosphere. While we agree on the use of a dipole field for shower development, we consider this as a too rough approximation for cutoff evaluation purposes. In ref.[ 14], which was meant to be mostly a demonstrative work and not a flux reference, a realistic description of geomagnetic field is chosen, but in order to make the calculus viable, “detector regions” were defined as large portions of the Earth’s surface.

We could not yet find a satisfactory solution, in terms of calculation power and precision at the same time, to include bending of charged particles during shower development. Therefore we have generated particles neglecting this aspect, while the field is accounted to determine the cutoff conditions for primary particles as seen by a specific detector location. This is performed according to the following procedure, which maximizes the use of the available information:

- neutrinos reaching the earth surface have been recorded with their impact position, energy, direction and with their primary cosmic ray position, energy, direction, charge and mass at the point of the first interaction in the atmosphere. No geomagnetic effect has been applied at this stage.
- Offline, all recorded neutrinos and their parents have been rotated in such a way to make their impact position correspond to the selected detector site. At the same time the corresponding upward going neutrino (and the position and direction of its parent primary cosmic ray) has been created out of simple geometrical considerations. Note please that at this stage the problem is still fully symmetric and

each downward going neutrino has a corresponding upward going one at the same location.

- The geomagnetic cutoff has been applied using standard techniques, making use of the information about the relative position and direction of the parent primary cosmic ray.

In this way we have been able to exploit all available statistics for each relevant detector site. On the other hand we are aware that neglecting bending of charged particles in atmosphere introduces some systematic errors. According to ref.[ 14] these should manifest themselves in particular observables, such as, for example, the East–West asymmetry. However it can be shown that we are talking of effects at the level of percent, which hardly affect the analysis of present neutrino events in terms of new physics. Therefore we prefer, for the moment, to account for this approximation in our systematic error budget (see section 7 ).

## 2.4. Solar Modulation

The cosmic ray spectrum depends on the phase of solar cycle. In order to modulate our primary spectrum, we adopt an algorithm proposed in ref.[ 15]. There the effect of solar modulation is treated in the framework of the “force field approximation”[ 16] which eventually express the modification of the spectrum as a function of energy as if due to an effective potential. For a given distance from the sun, this potential is a function only of time, and this has been parametrized as a function of the counting rate of the Climax neutron monitor[ 17], which has worked until year 2000. In this way we have evaluated the two extreme cases corresponding to average “minimum” and “maximum” solar activity. The algorithm adopted here is independent from those adopted in other authors’ works like those of ref. [ 18] and [ 11].

## 3. The Description of Hadronic Interactions

The hadronic packages of the FLUKA Monte Code are being developed according to a theoretically inspired approach, namely that interactions should be described in terms of the properties of elementary constituents. In principle one would like to derive all features of “soft” interactions (low- $p_T$  interactions) from the QCD Lagrangian, as it is done for hard processes. Unfortunately the large value taken by the running coupling constant prevents the use of the perturbative calculus. Indeed, in QCD, the color field acting among quarks is carried by the vector bosons of the strong interaction, the gluons, which are “colored” themselves. Therefore the characteristic feature of gluons (and QCD) is their strong self-interaction. If we imagine that quarks are held together by color lines of force, the gluon-gluon interaction will pull them together into the form of a tube or a string. Since quarks are confined, the energy required to “stretch” such a string is increasingly large until it suffices to materialize a quark-antiquark couple from the vacuum and the string breaks into two shorter ones, with still quarks at both ends. Therefore it is not unnatural that, because of quark confinement, theories based on interacting strings emerged as a powerful tool in understanding QCD at the soft hadronic scale (the non-perturbative regime). Different implementations of this idea exist, having obtained

remarkable success in describing the features of hadronic interactions. These concepts are embedded in FLUKA in order to give sound physical bases to each step.

It must be remarked that it is not yet possible to cover all relevant energy ranges by means of a unique numerical model. Different approaches are anyway required, and this imposes particular care so to have the proper matching and continuity at transition energies. Of course this point has been analysed in detail by FLUKA authors. In any case, a part the attention to the phenomenological aspects, the performances of the code are then optimized comparing with particle production data at single interaction level. The final predictions are obtained with a minimal set of free parameters, fixed for all energies and target/projectile combinations. Results in complex cases as well as scaling laws and properties come out naturally from the underlying physical models. The basic conservation laws are fulfilled “a priori”. This kind of approach has guaranteed a very high level of detail in FLUKA at least in principle. This is the reason why we propose its use when aiming at precision calculations with the idea of reaching a deeper understanding and reliability of predictions.

FLUKA contains two models to describe nonelastic hadronic interactions.

- The “low-intermediate” energy one, called PEANUT, which covers the energy range up to 5 GeV.
- The high energy one which can be used up to several tens of TeV, based on the color strings concepts sketched above.

The nuclear physics embedded in the two models is very much the same. The main differences are a coarser nuclear description (and no preequilibrium stage) and the Gribov-Glauber cascade for the high energy one.

### 3.1. The PEANUT Model

Hadron-nucleus non-elastic interactions are often described in the framework of the IntraNuclear Cascade (INC) models. These kind of models was developed at the very beginning of the history of energetic nuclear interaction modelling, but it is still valid and in some energy range it is the only available choice. Classical INC codes were based on a more or less accurate treatment of hadron multiple collision processes in nuclei, the target being assumed to be a cold Fermi gas of nucleons in their potential well. The hadron-nucleon cross sections used in the calculations are free hadron–nucleon cross sections. Usually, the only quantum mechanical concept incorporated was the Pauli principle. Possible hadrons were often limited to pions and nucleons, pions being also produced or absorbed via isobar (mainly  $\Delta_{33}$ ) formation, decay, and capture. Most of the historical weaknesses of INC codes have been mitigated or even completely solved in some of the most recent developments [20, 21], thanks to the inclusion of a so called “preequilibrium” stage, and to further quantistic effects including coherence and multibody effects.

All these improvements are considered in the PEANUT (PreEquilibrium Approach to NUclear Thermalization) model of FLUKA. Here the reaction mechanism is modelled in by explicit intranuclear cascade smoothly joined to statistical (exciton) preequilibrium emission [22] and followed by evaporation (or fission or Fermi break-up) and gamma deexcitation. In both stages, INC and exciton, the nucleus is modelled as a sphere with density given by a symmetrized Woods-Saxon [23] shape with parameters according to the

droplet model [ 24] for  $A > 16$ , and by a harmonic oscillator shell model for light isotopes (see [ 25]). The effects of the nuclear and Coulomb potentials outside the nuclear boundary are included. Proton and neutron densities are generally different. Binding energies are obtained from mass tables. Relativistic kinematics is applied at all stages, with accurate conservation of energy and momentum including those of the residual nucleus. Further details and validations can be found in [ 20].

For energies in excess of few hundreds MeV the inelastic channels (pion production channels) start to play a major role. The isobar model easily accommodates multiple pion production, for example allowing the presence of more than one resonance in the intermediate state (double pion production opens already at 600 MeV in nucleon-nucleon reactions, and at about 350 MeV in pion-nucleon ones). Resonances which appear in the intermediate states can be treated as real particles, that is, they can be transported and then transformed into secondaries according to their lifetimes and decay branching ratios.

### 3.2. The Dual Parton Model for high energy

A theory of interacting strings can be managed by means of the Reggeon-Pomeron calculus in the framework of perturbative Reggeon Field Theory[ 26], an expansion already developed before the establishment of QCD. Regge theory makes use explicitly of the constraints of analyticity and duality. On the basis of these concepts, calculable models can be constructed and one of the most successful attempts in this field is the so called “Dual Parton Model” (DPM), originally developed in Orsay in 1979 [ 27]. It provides the theoretical framework to describe hadron-nucleon interaction from several GeV onwards. DPM exhibited remarkable successes in predicting experimental observables. The quoted references include a vast amount of material showing the capabilities of the model when compared with experimental data. However, it must be stressed that other models are available, but most of them share an approach based on string formation and decay. For example, the *Quark Gluon String Model* [ 34] has been developed more or less in parallel with DPM, sharing most of the basic features of it.

In DPM a hadron is a low-lying excitation of an open string with quarks, antiquarks or diquarks sitting at its ends. In particular mesons are described as strings with their valence quark and antiquark at the ends. (Anti)baryons are treated like open strings with a (anti)quark and a (anti)diquark at the ends, made up with their valence quarks.

At sufficiently high energies, the leading term in high energy scattering corresponds to a “Pomeron” exchange (a closed string exchange with the quantum numbers of vacuum), which has a cylinder topology. By means of the optical theorem, connecting the forward elastic scattering amplitude to the total inelastic cross section, it can be shown that from the Pomeron topology it follows that two hadronic chains are left as the sources of particle production (unitarity cut of the Pomeron). While the partons (quarks or diquarks) out of which chains are stretched carry a net color, the chains themselves are built in such a way to carry no net color, or to be more exact to constitute color singlets like all naturally occurring hadrons. In practice, as a consequence of color exchange in the interaction, each colliding hadron splits into two colored system, one carrying color charge  $c$  and the other  $\bar{c}$ . These two systems carry together the whole momentum of the hadron. The system with color charge  $c$  ( $\bar{c}$ ) of one hadron combines with the system of complementary color of the other hadron, in such a way to form two color neutral chains. These chains appear as

two back-to-back jets in their own centre-of-mass systems. The exact way of building up these chains depends on the nature of the projectile-target combination (baryon-baryon, meson-baryon, antibaryon-baryon, meson-meson).

The single Pomeron exchange diagram is the dominant contribution, however higher order contributions with multi-Pomeron exchanges become important at energies in excess of 1 TeV in the laboratory. They correspond to more complicated topologies, and DPM provides a way for evaluating the weight of each, keeping into account the unitarity constraint. Every extra Pomeron exchanged gives rise to two extra chains which are built using two  $q\bar{q}$  couples excited from the projectile and target hadron sea respectively. The inclusion of these higher order diagrams is usually referred to as *multiple soft collisions*.

Two more ingredients are required to completely settle the problem. The former is the momentum distribution for the  $x$  variables of valence and sea quarks. Although the exact form of the momentum distribution function,  $P(x_1, \dots, x_n)$ , is not known, general considerations based on Regge arguments allow one to predict the asymptotic behavior of this distribution whenever each of its arguments goes to zero. The behavior turns out to be singular in all cases, but for the diquarks. A reasonable assumption, always made in practice, is therefore to approximate the true unknown distribution function with the product of all these asymptotic behaviors, treating all the rest as a normalization constant.

The latter ingredient is a hadronization model, which must take care of transforming each chain into a sequence of physical hadrons, stable ones or resonances. The basic assumption is that of *chain universality*, which assumes that once the chain ends and the invariant mass of the chain are given, the hadronization properties are the same regardless of the physical process which originated the chain. Therefore the knowledge coming from hard processes and  $e^+e^-$  collisions about hadronization can be used to fulfill this task. There are many more or less phenomenological models which have been developed to describe hadronization (examples can be found in [ 28, 29]). In principle hadronization properties too can be derived from Regge formalism [ 30].

It is possible to extend DPM to hadron-nucleus collisions too [ 27], making use of the so called Glauber-Gribov approach. Furthermore DPM provides a theoretical framework for describing hadron diffractive scattering both in hadron-hadron and hadron-nucleus collisions. General information on diffraction in DPM can be found in [ 31] and details as well as practical implementations in the DPM framework in [ 32].

At very high energies, those of interest for high energy cosmic ray studies ( $10\text{--}10^5$  TeV in the lab), hard processes can no longer be ignored. They are calculable by means of perturbative QCD and can be included in DPM through proper unitarization schemes which consistently treat soft and hard processes together.

### 3.3. Benchmarking of FLUKA hadronic models with experimental data

The predictions of FLUKA have been checked with a large set of experimental data collected in accelerator experiments. Reviews of these comparison with data can be found in [ 35]. Here we shall limit ourselves to show only a few examples, among the most important in view of the application of the code to cosmic ray applications.

Two sets of data are of particular relevance to check the quality of a model to be used for the calculation of atmospheric neutrino fluxes. These concern p-Be collisions and are reported in Fig. 2 and Fig. 3: in ref.[ 36] the central rapidity region has been



mainly explored, while in ref.[ 37] the forward region has been investigated. In both cases the agreement of FLUKA predictions is quite good. Measurements of  $\pi^\pm$  and  $K^\pm$  production rates by 400 GeV/c protons on Be targets were performed by Atherton et al. [ 38] for secondary particle momenta above 60 GeV/c and up to 500 MeV/c of transverse momentum. Recently the NA56/SPY (Secondary Particle Yields) experiment [ 39] was devoted to directly measure these yields in the momentum region below 60 GeV/c. The SPY experiment measured the production at different angles  $\theta$  and momenta  $P \leq 135$  GeV/c down to 7 GeV/c for pions, kaons, protons and their antiparticles, using a 450 GeV/c proton beam impinging on Be targets. These data were extremely valuable to improve the hadronization model of FLUKA so to arrive at the present version. FLUKA is in agreement with the Atherton *et al* and the SPY measurements at the level of  $\sim 20\%$  in the whole momentum range of all secondaries, with the exception of a few points mostly for negative kaons. The case of pions is reported in Fig. 4, and the analogous plot for kaons is given in Fig. 5. Also the  $\theta$  dependence of the measured yields is reasonably described by FLUKA. The measured  $K^\pm/\pi^\pm$  ratios are reproduced to better than 20% below 120 GeV/c.

#### 4. Features of nucleon-Air collisions in the FLUKA model

In the final state of one interaction one finds the fragments of the target nucleus, a leading nucleon that carries the baryon number of the projectile, a number of mesons, mostly pions, with a non negligible contribution of kaons. In addition one has to consider the production of nucleon antinucleon pairs and of heavy flavors, these effects are however of small importance at the energies that are relevant for atmospheric neutrinos. Most neutrinos are produced in the chain decay of the charged pions such as  $\pi^+ \rightarrow \mu^+ + \nu_\mu$  followed by  $\mu^+ \rightarrow e^+ \nu_e \bar{\nu}_\mu$  with  $K^\pm$  and  $K_L$  giving smaller contributions. In order to characterize the features of nucleon-Air collisions that are relevant in this discussion, we can identify few fundamental quantities: the nucleon-Air cross sections, the distribution of the energy fraction carried away by produced particles and the “spectrum weighted moments”  $Z_{ij}$ , all as a function of projectile energy.

In FLUKA, total, elastic and inelastic cross sections for hadron-Nucleus collisions are derived in the framework of the Glauber formalism, using as input the tabulated data (when they exist) of Particle Data Group for hadron-hadron collisions. In Fig. 6 we show the resulting proton-Air cross section for Nitrogen, Oxygen and Argon as a function of proton kinetic energy in the range 1-100 GeV (cross section for neutrons are very similar). We plot separately the elastic, inelastic and total contributions to cross section. Here what we call “inelastic” cross section is meant to include also what is usually called the “quasi-elastic” part, *i.e.* the one which corresponds to nuclear excitation without particle production.

The resulting interaction length in Air increases slowly and continuously from 85.1 g/cm<sup>2</sup> at about 5 GeV to 88.2 g/cm<sup>2</sup> at 100 GeV. Below 5 GeV the behavior is non monotonic due to the resonances effect, and the values varies between 81.9 and 85.1 g/cm<sup>2</sup>.

For our purposes, particle production can be conveniently studied in terms of a longitudinal non dimensional variable like  $x_{lab} = E_j/E_i$ , which is the ratio of the secondary

$E_k^p$ (GeV)	$\pi^+$	$\pi^-$	$\pi^0$	$K^+$	$K^-$	$K^0+K^{\bar{0}}$	$p$	$n$	$\Lambda$
5	0.149	0.092	0.150	0.0039	0.0001	0.0030	0.359	0.215	0.0066
10	0.157	0.112	0.163	0.0090	0.0014	0.0101	0.322	0.193	0.0141
30	0.161	0.124	0.172	0.0150	0.0056	0.0192	0.291	0.167	0.0179
50	0.162	0.128	0.175	0.0169	0.0079	0.0237	0.282	0.155	0.0185
100	0.166	0.134	0.180	0.0194	0.0116	0.0296	0.263	0.141	0.0181

Table 2

Average energy fractions of secondary particles produced in p–Air collisions as a function of the projectile kinetic energy.

particle  $j$  total energy over the primary particle  $i$  total energy ( $x_{lab}$  is approximately equal to  $x_F$  in the forward region). We can then construct the  $dN_{ij}/dx_{lab}$  distributions. These are the differential multiplicity distributions of secondary  $j$  as produced by primary  $i$  in collisions with Air nuclei as a function of  $x_{lab}$ . Examples of the  $x_{lab}$  distribution in p–Air collisions predicted by FLUKA are shown in Fig. 7, 8, 9, 10 and 11 respectively for produced  $\pi^+$ ,  $\pi^-$ ,  $K^+$ ,  $K^-$  and nucleons, at different kinetic energy of the projectile. Here  $x_{lab}$  is defined as the ratio of secondary total energy with respect to the primary total energy.

In table 2 we report the average energy fractions for the secondary particles, produced in proton–Air collisions, which mostly contribute to neutrino production, between 5 and 100 GeV of kinetic energy of the projectile in the laboratory system. Energy fraction is defined as:

$$F_{ij} = \int_0^1 x_{lab} \frac{dN_{ij}}{dx_{lab}} dx_{lab} \quad (2)$$

We also include  $\Lambda$ 's since they decay in a very short time, giving an effective contribution to pion production.

The numbers for neutron–Air collision are closely related, and, for the case of an isoscalar target, charge symmetry is substantially valid. Therefore, if we consider the production of a meson with isospin  $|I, I_z\rangle$ ,  $\langle E^{p+Air}(I_z) \rangle \simeq \langle E^{n+Air}(-I_z) \rangle$ , so that, for example,  $\langle E^{p+Air}(\pi^+) \rangle \simeq \langle E^{n+Air}(\pi^-) \rangle$ . This is relevant when nuclear primaries (even following the superposition principle) are considered, since their interaction is eventually reduced to Z proton–Air and A–Z neutron–Air collisions. We notice that these average energy fractions are approximately constant in this energy range, reflecting an approximate validity of Feynman scaling in the model. At low  $E_{kin}$  (few GeV's), only pions are significantly produced, but their energy fraction decreases: this is a reflection of the fact that an approximately constant amount of energy  $\Delta E_{frag}$  is absorbed in the excitation of the target nucleus, and with decreasing projectile energy this represents a larger and larger contribution to the average energy fraction.

The spectrum weighted moments are defined as:

$$Z_{ij} = \int_0^1 (x_{lab})^{\gamma-1} \frac{dN_{ij}}{dx_{lab}} dx_{lab} \quad (3)$$

$E_k^p$ (GeV)	$\pi^+$	$\pi^-$	$K^+$	$K^-$	$p+n$
5	0.0388	0.0229	0.0012	0.0000	0.374
10	0.0404	0.0271	0.0026	0.0003	0.330
30	0.0415	0.0306	0.0042	0.0015	0.294
50	0.0422	0.0315	0.0048	0.0022	0.282
100	0.0426	0.0327	0.0052	0.0030	0.261

Table 3

Spectrum weighted moments (for a spectral index of the differential primary spectrum  $\gamma=2.7$ ) for secondary particles produced in p–Air collisions as a function of the projectile kinetic energy.

where  $\gamma = 2.7$  is the approximate spectral index of the differential cosmic ray spectrum. Their use in the literature is justified by the fact that the inclusive yield of secondary cosmic ray particles at a given energy is almost proportional to  $Z$ , when the primary spectrum is a power law with a constant spectral index in the whole useful energy spectrum. This is a good approximation for nucleon energies exceeding the TeV scale, but it is not the case in the range of energies considered in this work, since a single power law does not fit the primary spectrum. However, they remain a useful and commonly accepted tool to characterize and compare different interaction models (notice that for  $\gamma=2$  they reduce to the energy fractions). For instance, we can state that, in a first approximation, the flux of  $\nu_\mu + \bar{\nu}_\mu$  from pions only (excluding for instance muon decay) can be considered as:

$$\phi_{\nu_\mu + \bar{\nu}_\mu} \propto \frac{Z_{p\pi^+} + Z_{p\pi^-}}{1 - Z_{pp} - Z_{pn}} \quad (4)$$

The resulting spectrum weighted moments are tabulated in Table 3.

## 5. Example of calculations of particles in atmosphere

Beyond the topic of atmospheric neutrino fluxes, the FLUKA interaction model has been used also to produce results on other secondary particles produced in atmosphere by cosmic rays, which can be used as further cross check of the validity of the model. At least two remarkable results can be quoted:

1. The reproduction of the features of primary proton flux as a function of geomagnetic latitude as measured by AMS[ 40], thus showing that the geomagnetic effects and the overall geometrical description of the 3–D setup are well under control[ 41]. In addition, the same work shows that also the fluxes of secondary  $e^+e^-$  measured at high altitude are well reproduced. Sub-cutoff  $e^\pm$  are mainly (97%) coming from decays of pions produced in the proton collisions with the atmospheric nuclei: charged pions contribute through the  $\pi - \mu - e$  chain, while  $\pi^0$  through  $\pi^0 \rightarrow \gamma \gamma$  with subsequent e.m. showers. The relative contribution of charged pions to the sub-cutoff electrons (positron) fluxes at AMS altitude is found to be 37% (47%), while the remaining 60% (50%) appears to come from  $\pi^0$  production. This point

deserves some considerations. The level of agreement in the comparison of data and predictions for  $e^\pm$  fluxes turns out to be an important benchmark for the interaction model from the point of view of particle production in atmosphere, since it is strictly linked to the meson production (mostly pions at this energy).

2. The good reproduction of the data on muons in atmosphere as measured by the CAPRICE experiment[ 42], both at ground level and at different floating altitudes: see ref.[ 43] for the relevant plots and numbers. The agreement exhibited by the FLUKA simulation for muons of both charges gives confidence on the predictions of FLUKA for the parent mesons of muons (mostly pions). This work complements the previously mentioned studies oriented to the validation of the model in terms of particle yields.

The fluxes of atmospheric muons are strictly related to the neutrino ones, because almost all  $\nu$ 's are produced either in association, with, or in the decay of  $\mu^\pm$ . Therefore it is possible to conclude that, for that choice of primary spectrum, the  $\nu$  fluxes predicted by FLUKA are probably in the right range. In the last years it has been remarked the noticeable agreement between the original HKKM[ 18] and Bartol[ 11] calculations of the  $\nu$  fluxes, despite they started from different estimates of the primary flux and different hadronic interaction models. Probably such an agreement is not casual, but the result of the  $\mu$  constraint, producing a sort of error compensation. If that is the case, the resulting flux could be biased by some systematics.

The shower simulations in atmosphere with FLUKA have been compared also to the most recent hadron spectra at different latitudes and altitudes, obtaining remarkable agreement. As an example, in fig. 12 we compare MonteCarlo results to the hadron flux referred to the vertical as measured with the calorimeter of the KASCADE experiment[ 44, 45] with two different angular acceptances.

## 6. Simulation Results

In Tables 4, 5, 6 and 7 we give the differential  $\nu_e$ ,  $\bar{\nu}_e$ ,  $\nu_\mu$  and  $\bar{\nu}_\mu$  flux in units  $\text{cm}^{-2} \text{s}^{-1} \text{sr}^{-1} \text{GeV}^{-1}$  for some energy and cosine of the zenith angle bins. The tables are given for Super-Kamiokande site and solar maximum, having used the average primary cosmic ray fit in [ 12]. The full tables with a total number of 40 angular bins between  $\cos\theta = -1$  to 1 and 68 energy bins between 0.1 and 200 GeV are accessible in [ 8], together with the similar tables for Soudan and Gran Sasso cut-offs.

In Fig. 13, 14, 15 and 16 the differential flux as a function of neutrino energy is shown for some values of  $\cos\theta$  at Super-Kamiokande site and solar maximum for the 4 flavors. A characteristic feature of the 3-D calculation is the excess of events from near the horizontal at low energy. This was shown clearly in the first FLUKA paper[ 7]. Such a feature is clearly maintained in the plots reported here. Additional explanations of how this effect originates are given in [ 14].

Fig. 17 shows the angle averaged over the lower hemisphere differential electron neutrino and anti-neutrino fluxes multiplied by  $E^{2.5}$  at Super-Kamiokande for both solar minimum and solar maximum modulation.

In order to give a comparison with respect to the calculation referenced so far by current experiments, the FLUKA flux is shown together with the Bartol group flux [ 11] (dotted and red line) and the HKKM [ 46] (dashed and green line). It should be considered that, while the FLUKA flux has been derived using the new fit to recent primary cosmic ray measurements, the Bartol and HKKM fluxes were calculated using different evaluations of the primary fluxes. It can be noticed that in our case the difference in flux due to solar modulation is much more limited than for Bartol calculation. Our minimum/maximum ratio is much closer to that of HKKM flux.

Fig. 18 shows the same comparison but for muon neutrinos and anti-neutrinos. It has to be mentioned that both Bartol and the Japanese group are working to improve their predictions. A part from the update of the primary flux compilation, Bartol is also improving their interaction model, as preliminary described in ref.[ 47], while Honda and co-workers are now using DPMJET-III[ 48], and their new results are reported in [ 52, 19]. There they also introduce the 3-D geometry, and the geomagnetic field is included, although in the dipole approximation, also during shower development. These new results, included the Bartol one, predict (at least for the Super-Kamiokande site) a lower flux normalization, now closer to the FLUKA one, with respect to the previous references of [ 11] and [ 18].

In Fig. 19 we show the quantity  $R = \Phi(\text{new CR flux})/\Phi(\text{old CR flux})$  calculated making the ratio of the solid angle averaged FLUKA muon neutrino plus antineutrino flux as a function of neutrino energy for the calculation reported here (i.e. using the new fit to recent primary cosmic ray measurements) over the flux as resulting from our previous calculation, where the same primary flux as in Ref. [ 11] was used. The ratio  $R$  is shown at Super-Kamiokande site and for solar maximum and minimum. The band shows the region between the maximum and minimum fit which can be obtained from the measurements used. In Fig. 20 the same ratios are shown for Soudan (low cut-off) site. The same plots for electron neutrinos are not shown because they are very similar to those for muon neutrinos. Notice the ratio represents the effect of changing the primary cosmic ray spectrum in a neutrino flux calculation, because no other main ingredient was changed between the newer and older results. It can be noticed that the improved estimate of the primary cosmic flux will increase predictions of the order of 15% for the Sub-GeV events, while for Multi-GeV and through-going muons new predictions should be about 20% lower in normalization.

## 7. Estimate of Systematic Errors

Uncertainties in the flux of atmospheric neutrinos are presently attributed mostly to the primary spectrum and to the treatment of hadronic interactions. In addition, there are minor uncertainties related to the details of shower calculation (atmosphere, technical algorithms, etc.).

As far as the primary spectrum is concerned, trusting the uncertainty on the fit of [ 12], we derive from Fig. 19 and 20 that this translates into an uncertainty of about  $\pm 7\%$ , up to 100 GeV.

$\phi(\nu_e)$	Cosine of zenith angle											
$E_\nu$ (GeV)	-0.975	-0.825	-0.625	-0.425	-0.225	-0.025	0.025	0.225	0.425	0.625	0.825	0.975
0.106	0.25	0.28	0.31	0.30	0.40	0.67	0.67	0.29	0.21	0.18	0.17	0.17
0.168	0.16	0.18	0.19	0.18	0.22	0.35	0.35	0.17	0.13	0.12	0.11	0.11
0.299	0.71E-01	0.77E-01	0.82E-01	0.76E-01	0.86E-01	0.12	0.12	0.70E-01	0.60E-01	0.56E-01	0.53E-01	0.51E-01
0.531	0.24E-01	0.26E-01	0.28E-01	0.26E-01	0.29E-01	0.38E-01	0.38E-01	0.25E-01	0.23E-01	0.21E-01	0.19E-01	0.19E-01
0.944	0.62E-02	0.67E-02	0.74E-02	0.75E-02	0.83E-02	0.99E-02	0.99E-02	0.79E-02	0.70E-02	0.62E-02	0.56E-02	0.53E-02
1.679	0.13E-02	0.14E-02	0.16E-02	0.18E-02	0.21E-02	0.24E-02	0.24E-02	0.21E-02	0.18E-02	0.15E-02	0.13E-02	0.12E-02
2.985	0.21E-03	0.24E-03	0.30E-03	0.36E-03	0.46E-03	0.56E-03	0.56E-03	0.47E-03	0.37E-03	0.29E-03	0.24E-03	0.21E-03
5.309	0.34E-04	0.40E-04	0.50E-04	0.67E-04	0.95E-04	0.12E-03	0.12E-03	0.95E-04	0.67E-04	0.50E-04	0.39E-04	0.33E-04
9.441	0.45E-05	0.52E-05	0.70E-05	0.10E-04	0.16E-04	0.24E-04	0.24E-04	0.16E-04	0.10E-04	0.70E-05	0.52E-05	0.45E-05
16.788	0.57E-06	0.68E-06	0.91E-06	0.14E-05	0.23E-05	0.41E-05	0.41E-05	0.23E-05	0.14E-05	0.91E-06	0.68E-06	0.57E-06
29.854	0.70E-07	0.85E-07	0.11E-06	0.17E-06	0.32E-06	0.64E-06	0.64E-06	0.32E-06	0.17E-06	0.11E-06	0.85E-07	0.70E-07
53.088	0.80E-08	0.10E-07	0.14E-07	0.20E-07	0.41E-07	0.90E-07	0.90E-07	0.41E-07	0.20E-07	0.14E-07	0.10E-07	0.80E-08
94.406	0.85E-09	0.11E-08	0.16E-08	0.23E-08	0.51E-08	0.11E-07	0.11E-07	0.51E-08	0.23E-08	0.16E-08	0.11E-08	0.84E-09
167.880	0.79E-10	0.10E-09	0.19E-09	0.25E-09	0.62E-09	0.12E-08	0.12E-08	0.62E-09	0.25E-09	0.19E-09	0.11E-09	0.81E-10

Table 4: Electron neutrino flux ( $\text{cm}^2 \text{ s sr GeV}^{-1}$ ) as a function of energy for different values of the cosine of zenith angle as calculated for the Super-Kamiokande site for maximum solar modulation.

$\phi(\bar{\nu}_e)$	Cosine of zenith angle											
$E_\nu$ (GeV)	-0.975	-0.825	-0.625	-0.425	-0.225	-0.025	0.025	0.225	0.425	0.625	0.825	0.975
0.106	0.23	0.25	0.27	0.27	0.36	0.65	0.65	0.28	0.20	0.18	0.17	0.16
0.168	0.14	0.15	0.16	0.16	0.19	0.32	0.32	0.16	0.12	0.11	0.11	0.10
0.299	0.62E-01	0.65E-01	0.70E-01	0.65E-01	0.75E-01	0.11	0.11	0.64E-01	0.55E-01	0.51E-01	0.49E-01	0.47E-01
0.531	0.20E-01	0.21E-01	0.23E-01	0.22E-01	0.25E-01	0.33E-01	0.33E-01	0.23E-01	0.20E-01	0.19E-01	0.17E-01	0.16E-01
0.944	0.51E-02	0.54E-02	0.61E-02	0.62E-02	0.70E-02	0.84E-02	0.84E-02	0.68E-02	0.60E-02	0.54E-02	0.48E-02	0.45E-02
1.679	0.10E-02	0.11E-02	0.13E-02	0.14E-02	0.17E-02	0.20E-02	0.20E-02	0.17E-02	0.15E-02	0.12E-02	0.10E-02	0.96E-03
2.985	0.17E-03	0.19E-03	0.23E-03	0.28E-03	0.37E-03	0.45E-03	0.45E-03	0.38E-03	0.29E-03	0.23E-03	0.19E-03	0.17E-03
5.309	0.27E-04	0.31E-04	0.39E-04	0.50E-04	0.74E-04	0.93E-04	0.93E-04	0.74E-04	0.50E-04	0.38E-04	0.31E-04	0.26E-04
9.441	0.35E-05	0.42E-05	0.54E-05	0.74E-05	0.13E-04	0.18E-04	0.18E-04	0.13E-04	0.74E-05	0.54E-05	0.42E-05	0.35E-05
16.788	0.45E-06	0.56E-06	0.71E-06	0.10E-05	0.20E-05	0.34E-05	0.34E-05	0.20E-05	0.10E-05	0.71E-06	0.56E-06	0.45E-06
29.854	0.54E-07	0.67E-07	0.87E-07	0.13E-06	0.26E-06	0.58E-06	0.58E-06	0.26E-06	0.13E-06	0.87E-07	0.67E-07	0.54E-07
53.088	0.62E-08	0.69E-08	0.10E-07	0.15E-07	0.32E-07	0.90E-07	0.90E-07	0.32E-07	0.15E-07	0.10E-07	0.69E-08	0.62E-08
94.406	0.64E-09	0.61E-09	0.12E-08	0.16E-08	0.38E-08	0.12E-07	0.12E-07	0.38E-08	0.16E-08	0.12E-08	0.61E-09	0.64E-09
167.880	0.60E-10	0.46E-10	0.14E-09	0.16E-09	0.44E-09	0.15E-08	0.15E-08	0.44E-09	0.16E-09	0.14E-09	0.46E-10	0.60E-10

Table 5: Electron anti-neutrino flux ( $\text{cm}^2 \text{ s sr GeV}^{-1}$ ) as a function of energy for different values of the cosine of zenith angle as calculated for the Super-Kamiokande site for maximum solar modulation.

$\phi(\nu_\mu)$	Cosine of zenith angle											
$E_\nu$ (GeV)	-0.975	-0.825	-0.625	-0.425	-0.225	-0.025	0.025	0.225	0.425	0.625	0.825	0.975
0.106	0.51	0.56	0.62	0.62	0.81	1.5	1.5	0.60	0.43	0.37	0.35	0.34
0.168	0.33	0.35	0.38	0.35	0.43	0.71	0.71	0.34	0.26	0.24	0.23	0.23
0.299	0.15	0.15	0.16	0.14	0.16	0.24	0.24	0.14	0.12	0.11	0.11	0.11
0.531	0.51E-01	0.52E-01	0.54E-01	0.49E-01	0.53E-01	0.69E-01	0.69E-01	0.48E-01	0.44E-01	0.42E-01	0.41E-01	0.41E-01
0.944	0.14E-01	0.14E-01	0.15E-01	0.14E-01	0.15E-01	0.18E-01	0.18E-01	0.15E-01	0.14E-01	0.13E-01	0.13E-01	0.12E-01
1.679	0.33E-02	0.33E-02	0.35E-02	0.35E-02	0.37E-02	0.43E-02	0.43E-02	0.38E-02	0.36E-02	0.33E-02	0.32E-02	0.31E-02
2.985	0.68E-03	0.70E-03	0.74E-03	0.78E-03	0.86E-03	0.97E-03	0.97E-03	0.89E-03	0.80E-03	0.74E-03	0.70E-03	0.68E-03
5.309	0.14E-03	0.15E-03	0.16E-03	0.17E-03	0.20E-03	0.21E-03	0.21E-03	0.19E-03	0.16E-03	0.15E-03	0.14E-03	0.14E-03
9.441	0.26E-04	0.27E-04	0.28E-04	0.32E-04	0.37E-04	0.41E-04	0.41E-04	0.37E-04	0.32E-04	0.28E-04	0.27E-04	0.26E-04
16.788	0.48E-05	0.51E-05	0.51E-05	0.60E-05	0.71E-05	0.76E-05	0.76E-05	0.71E-05	0.60E-05	0.52E-05	0.51E-05	0.48E-05
29.854	0.85E-06	0.89E-06	0.93E-06	0.11E-05	0.13E-05	0.14E-05	0.14E-05	0.13E-05	0.11E-05	0.94E-06	0.89E-06	0.85E-06
53.088	0.14E-06	0.14E-06	0.16E-06	0.18E-06	0.22E-06	0.24E-06	0.24E-06	0.22E-06	0.18E-06	0.16E-06	0.14E-06	0.14E-06
94.406	0.20E-07	0.21E-07	0.24E-07	0.28E-07	0.34E-07	0.39E-07	0.39E-07	0.34E-07	0.28E-07	0.24E-07	0.21E-07	0.20E-07
167.880	0.27E-08	0.27E-08	0.33E-08	0.41E-08	0.47E-08	0.60E-08	0.60E-08	0.46E-08	0.42E-08	0.33E-08	0.27E-08	0.27E-08

Table 6: Muon neutrino flux ( $\text{cm}^2 \text{ s sr GeV}^{-1}$ ) as a function of energy for different values of the cosine of zenith angle as calculated for the Super-Kamiokande site for maximum solar modulation.



$\phi_{\bar{\nu}_\mu}$	Cosine of zenith angle											
$E_\nu$ (GeV)	-0.975	-0.825	-0.625	-0.425	-0.225	-0.025	0.025	0.225	0.425	0.625	0.825	0.975
0.106	0.51	0.56	0.62	0.60	0.81	1.4	1.4	0.60	0.43	0.38	0.35	0.35
0.168	0.33	0.35	0.38	0.35	0.43	0.69	0.69	0.34	0.26	0.24	0.23	0.23
0.299	0.15	0.15	0.16	0.14	0.16	0.24	0.24	0.14	0.12	0.11	0.11	0.11
0.531	0.50E-01	0.51E-01	0.53E-01	0.49E-01	0.52E-01	0.68E-01	0.68E-01	0.47E-01	0.43E-01	0.42E-01	0.41E-01	0.40E-01
0.944	0.13E-01	0.14E-01	0.14E-01	0.14E-01	0.15E-01	0.18E-01	0.18E-01	0.14E-01	0.13E-01	0.13E-01	0.12E-01	0.12E-01
1.679	0.30E-02	0.31E-02	0.33E-02	0.33E-02	0.36E-02	0.42E-02	0.42E-02	0.37E-02	0.34E-02	0.31E-02	0.29E-02	0.28E-02
2.985	0.59E-03	0.62E-03	0.67E-03	0.72E-03	0.84E-03	0.97E-03	0.97E-03	0.86E-03	0.74E-03	0.67E-03	0.62E-03	0.59E-03
5.309	0.12E-03	0.12E-03	0.13E-03	0.15E-03	0.18E-03	0.21E-03	0.21E-03	0.18E-03	0.14E-03	0.13E-03	0.12E-03	0.12E-03
9.441	0.20E-04	0.22E-04	0.24E-04	0.27E-04	0.33E-04	0.45E-04	0.45E-04	0.33E-04	0.27E-04	0.24E-04	0.22E-04	0.20E-04
16.788	0.35E-05	0.38E-05	0.42E-05	0.48E-05	0.58E-05	0.86E-05	0.86E-05	0.58E-05	0.48E-05	0.43E-05	0.38E-05	0.35E-05
29.854	0.60E-06	0.65E-06	0.72E-06	0.82E-06	0.10E-05	0.15E-05	0.15E-05	0.10E-05	0.81E-06	0.71E-06	0.65E-06	0.60E-06
53.088	0.97E-07	0.11E-06	0.11E-06	0.13E-06	0.17E-06	0.23E-06	0.23E-06	0.17E-06	0.13E-06	0.11E-06	0.11E-06	0.97E-07
94.406	0.15E-07	0.16E-07	0.15E-07	0.20E-07	0.28E-07	0.31E-07	0.31E-07	0.29E-07	0.20E-07	0.15E-07	0.17E-07	0.15E-07
167.880	0.21E-08	0.23E-08	0.19E-08	0.29E-08	0.45E-08	0.38E-08	0.38E-08	0.47E-08	0.30E-08	0.19E-08	0.24E-08	0.21E-08

Table 7: Muon anti-neutrino flux ( $\text{cm}^2 \text{ s sr GeV}^{-1}$ ) as a function of energy for different values of the cosine of zenith angle as calculated for the Super-Kamiokande site for maximum solar modulation.

The attribution of a systematic error to the hadronic interaction model is difficult, since there is not the possibility of comparing predictions to experimental data in the whole phase space of interest. The existing data point out that, on average, the agreement of FLUKA predictions of data is at the level of about 10%. In some limited region of phase space the level of agreement might be worse, although not above 20%. In the recent years, a lot of work has been done instead to compare different models to establish a sort of relative uncertainty. If we consider in the comparison the first models adopted by Bartol and Honda et al., differences of the order of  $\pm 20$  to 25% have been found, at least for the range of energy considered in this paper. In our opinion this is not to be considered as a correct estimate of the overall theoretical uncertainty, but instead a measurement of the insufficient accuracy of the first models. Indeed, the recent developments and upgrades are converging towards a narrower uncertainty interval, which we estimate not larger than  $\pm 10$  to 15%. The Sub-GeV region of atmospheric neutrinos seems the one where the theoretical uncertainty appears to be dominant, and this reflects the poor knowledge of particle productions in nucleon–Nucleus interaction at few GeV's. Recently, we have also made preliminary investigations of the possible error introduced by assuming the validity of the superposition model[ 49], by testing a preliminary interface to DPMJET-II.5[ 50] inside FLUKA to perform the explicit nucleus-nucleus Nucleus-Air interaction. The results do not show any significant deviation from those obtained with the superposition model, in contrast to what instead is claimed in ref.[ 51].

In any case, the predictions on flavor ratio, which is an essential element for the analysis of neutrino data in terms of new physics (oscillations), have always been much less dependent on the hadronic model:  $\pm 2$  to 5%. As a first approximation, the main source of uncertainty in the prediction of the standard-model  $\mu/e$  ratio comes from the difference between  $\pi^+$  and  $\pi^-$ . The decay of  $\pi^+$  eventually results in  $\nu_e$  while the decay of  $\pi^-$  generates  $\bar{\nu}_e$ ; in both cases a pair  $(\nu_\mu, \bar{\nu}_\mu)$  is also produced.

About other sources of uncertainties, the most relevant seem to be the choice of an average atmosphere and the common practice of neglecting mountain shapes for the prediction in specific sites. As far as the atmosphere is concerned, we agree that pressure and density variations may have a noticeable impact on muon fluxes, and mostly at ground level. For neutrinos these turn out to be much less important, since the effect is averaged over many directions, and we estimated a contribution not larger than 1% (up to 100 GeV of neutrino energy).

In our calculation we have not yet introduced the geomagnetic field during shower development in atmosphere. From a set of small scale tests, we expect that this might have brought to an overestimate of the absolute flux by few percent. Furthermore, we also know that this choice would produce a non correct east–west asymmetry, as compared with data.

The previous considerations can be used to provide an overall estimate of the theoretical uncertainty of the present calculation. Taking 7% for the primary spectrum, 15% for the interaction model, 1% for the atmosphere and 2% for the geomagnetic field and combining them in quadrature, a total of 17% is obtained.

As a last remark, we want to state that, as far as the comparison with experimental data on atmospheric neutrinos are concerned, another important source of uncertainty must be included, that is the one associated to neutrino–Nucleus cross section.

## 8. Conclusions

The first phase of atmospheric neutrino flux calculation using the FLUKA code is here concluded. We think that these results, apart from the question of the 3-D geometry, assessed already in [ 7], represent the first systematic attempt to explore the impact of a refined hadronic interaction model, which is capable at the same time to reproduce a wide range of accelerator and cosmic ray data. This work has stimulated a serious debate inside the scientific community about the validity of the previous “traditional” calculations, and we consider the recent convergence towards a lower normalization of neutrino fluxes (for the same or similar primary spectrum) as an important achievement and recognition of the importance of using accurate interaction models for cosmic ray calculations. Along this line other attempts have been followed, like the works of ref.[ 53, 51, 54, 55, 56]. Some of these attempts are, in our opinion, biased again by the choice of interaction models which are not precise. In particular we refer to those which are based upon the use of the old GHEISHA model[ 57], a parametrized code which fails in giving proof of reliability in reproducing particle production properties, as recently shown for instance in the framework of ALICE experiment at LHC[ 58]. The calculation of ref.[ 53], which is based on GEANT-FLUKA, cannot be compared to ours, since the FLUKA package contained in GEANT-3 is an old and incomplete version of the present FLUKA. In particular it does not contain the fundamental PEANUT section and the high energy part (above 5 GeV) is now considered obsolete. The work of ref.[ 56] is instead originally biased by a technical error in the normalization, as recently communicated by the author[ 60].

As mentioned above, these results cannot yet be considered as completely final, since we are aware that a fully certified calculation must include the geomagnetic field also during shower development. However this has to be done using the most accurate description of this field, avoiding approximations, and this will be the object of our next development. Furthermore, the calculation of neutrino fluxes is also going to be extended at higher energies, as soon as it will be released a next extension of the FLUKA model in order to deal with nucleus–nucleus interactions up to extreme high energies[ 61].

The importance of reducing as much as possible the theoretical uncertainties in the calculation of these fluxes may have limited impact in the analysis of present experimental results concerning neutrino oscillations where normalization is left as a free parameter so that results are not dependent on it. The matter can be different in the framework of a 3–flavor scenario, where sub-GeV electron neutrinos acquire some weight: there in fact, one expects to see the effects of interference terms involving  $\theta_{12}$ , if the LMA solution for solar neutrino turns out to be the right one, as confirmed by the recent SNO results[ 59]. From the experimental point of view, the ICARUS experiment could be the one who can investigate with low or negligible systematic error the sector of low energy electron neutrinos in the atmospheric flux.

## Acknowledgments

We wish to thank Prof. C. Rubbia, the Icarus collaboration and the MACRO collaboration for the strong support to this effort. We acknowledge the fruitful discussions with R. Engel, T.K. Gaisser, M. Honda, T. Kajita, P. Lipari, V. Naumov, T. Stanev

and F. Villante. The Bartol group provided us the primary spectrum fit. The Super-Kamiokande collaboration, through Dr. Choji Saji, provided us with the HKKM tables of angle integrated fluxes.

## REFERENCES

1. The Super-Kamiokande Coll. (Y. Fukuda et al.), Phys. Rev. Lett. **81** (1998) 1562.
2. The MACRO Coll. (M. Ambrosio et al.), Phys. Lett. **B434** (1998), 451, hep-ex/9807005
3. The Soudan2 Coll. (W.W.M. Allison et al.), Phys. Lett. **B449** (1999) 137.
4. A. Ferrari and P.R. Sala, ATLAS internal note ATL-PHYS- 97-113 (1997) accessible through the CERN preprint server; Proc. of the *Workshop on Nuclear Reaction Data and Nuclear Reactors Physics, Design and Safety*, ICTP, Miramare-Trieste, Italy, 15 April–17 May 1996, Proceedings published by World Scientific, A. Gandini, G. Reffo eds, Vol. 2, p. 424, (1998).
5. G. Battistoni et al., Nuclear Phys. B (Proc. Suppl.) **70** (1998) 358.
6. P. Cennini et al. (ICARUS coll.) ICARUS II, Experiment proposal Vol. I & II, LNGS-94/99-I&II
7. G. Battistoni et al., Astrop. Phys. **12** (2000) 315.
8. FLUKA flux tables are available at <http://www.mi.infn.it/~battist/neutrino.html>.
9. The fit to atmospheric profile has been taken from T. K. Gaisser, “Cosmic Rays and Particle Physics”, Cambridge University Press, Cambridge, England. It has to be noticed that, the second term of Eq. 3.22 has a wrong sign because of a misprinting error.
10. see <http://nssdc.gsfc.nasa.gov/space/model/atmos/cospar1.html>
11. G. Barr et al., Phys. Rev. **D39** (1989) 3532; V. Agrawal, T.K. Gaisser, P. Lipari and T. Stanev, Phys. Rev. **D53** (1996) 1314.
12. T.K. Gaisser, M. Honda, P. Lipari and T. Stanev, Primary spectrum to 1 TeV and beyond, OG1.01, Proceedings of 27<sup>th</sup> International Cosmic Ray Conference, Hamburg (2001).
13. <http://nssdc.gsfc.nasa.gov/space/model/models/igrf.html>
14. P. Lipari, Astrop. Phys. **14** (2001) 1038.
15. G.D. Badhwar and P.M. O’Neill, Adv. Space Res. Vol. **17**, No. 2 (1996) 7.
16. L.J. Gleason and W.I. Axford, Astrophys. J. **149** (1967) L115 and **154** (1968) 1011.
17. <http://ulysses.uchicago.edu/NeutronMonitor/Misc/neutron2.html>
18. M. Honda et al., Phys. Rev. **D52** (1995) 4985.
19. M. Honda, T. Kajita, K. Kasahara and S. Midorikawa, Phys. Rev. **D64** (2001) 053011.
20. A. Fassò, A. Ferrari, J. Ranft, P.R. Sala, *FLUKA: Status and Prospective for Hadronic Applications*, invited talk in Proceedings of the MonteCarlo 2000 Conference, Lisbon, October 23–26 2000, A. Kling, F. Barão, M. Nakagawa, L. Távora, P. Vaz eds., Springer-Verlag Berlin, p. 955-960 (2001). Other references and documentation on FLUKA are available at <http://www.fluka.org>
21. S.G. Mashnik and S.A. Smolyansky, *The cascade-exciton approach to nuclear reactions: foundation and achievements*, JINR preprint 1994: E2-94-353; R.E. Prael and M. Bozoian, *Adaptation of the Multistage Preequilibrium model for the MonteCarlo*

- Method (I)*, Los Alamos report 1988: LA-UR-88-3238.
22. E. Gadioli and P. E. Hodgson, *Pre-equilibrium Nuclear Reactions*, Clarendon Press, Oxford, (1992).
  23. M.E. Grypeos et al., J. Phys. **G 17** (1991) 1093.
  24. W.D. Myers, *Droplet Model of Atomic Nuclei*, IFI/Plenum, New York, 1977.
  25. L.R.B. Elton, *Nuclear sizes*, Oxford University Press, 1961.
  26. For a review of Regge theory applied to high energy scattering see P.D.B. Collins, *An Introduction to Regge Theory & High Energy Physics*, (Cambridge University Press, Cambridge 1977).
  27. A. Capella et al., Z. Phys. **C3**, 329 (1980); A. Capella, and J. Tran Thanh Van, Phys. Lett. **B93**, 146 (1980); A. Capella et al., Phys. Rep. **236**, 225 (1994).
  28. T. Sjostrand, CERN Report CERN-TH 6488/92 (1992).
  29. S. Ritter, *Comput. Phys. Commun.* 31, 393 (1984); J. Ranft, and S. Ritter, Acta Phys. Pol. **B11** 259 (1980).
  30. A.B. Kaidalov, and O.I. Piskunova, Z. Phys. **C30**, 141 (1986); A. Capella et al., Z. Phys. **C70**, 507 (1996).
  31. K. Goulianos, Phys. Rep. **101**, 169 (1983).
  32. S. Roesler et al., Z. Phys. **C59**, 481 (1993); J. Ranft, and S. Roesler, Z. Phys. **C62**, 329 (1994).
  33. K. Hahn, and J. Ranft, Phys. Rev. **D41**, 1463 (1990); F.W. Bopp et al., Phys. Rev **D49**, 3236 (1994); P. Aurenche et al., Phys. Rev **D45**, 92 (1992).
  34. A. Kaidalov, Phys. Lett. **B117**, 459 (1982); A. Kaidalov, and K.A. Ter-Martirosyan, *Phys. Lett.* B117, 247 (1982).
  35. For a wide review of FLUKA benchmarks, see Proc. of the 1st International Workshop on Space Radiation Research and 11th NASA Space Radiation Health Investigators Workshop, Arona, Italy, May 2000.
  36. T. Abbott et al Phys. Rev. **D45(11)**, 3906 (1992)
  37. T. Eichten et al. Nucl. Phys. **B44**, 333 (1972).
  38. H.W. Atherton, CERN 80-07 (1980).
  39. G. Ambrosini et al., Phys. Lett. **B425** 208 (1988).
  40. J.Alcaraz et al.,AMS Collaboration, Cosmic Protons, Phys. Lett. **B490**, (2000) 27.
  41. P. Zuccon et al., Proc. of Taup 2001, Sep. 8-12 2001, Assergi, Italy. Also: astro-ph/0111111.
  42. M. Boezio et al., Phys. Rev. **D62** (2000) 032007.
  43. G. Battistoni et al., Astrop. Phys. **17** (2002) 477, also hep-ph/0107241
  44. H.H Mielke et al., *Cosmic ray hadron flux at sea level up to 15 TeV*, Journ. Phys. G **20** (1994) 637-650
  45. H. Kornmayer et al, *High-energy cosmic-ray neutrons at sea level*, Journ. Phys. G**21** (1995) 439-450.
  46. The HKKM fluxes tabulated for different modulations have been provided by the Super-Kamiokande group (Dr. Choji Saji).
  47. T.K. Gaisser, Proc. of Taup 2001, Sep. 8-12 2001, Assergi (Italy); R. Engel, T.K. Gaisser, P. Lipari & T. Stanev, Proc. of the 27th Int. Cosmic Ray Conf., Hamburg 4 (2001) 1381.
  48. Roesler S, Engel & R, Ranft J. Proc. of the 27th Int. Cosmic Ray Conf., Hamburg, 1

- (2001) 439, Phys. Rev. **D57** (1998) 2889, **D55** (1997) 6957.
49. G. Battistoni et al., *Progresses in the validation of the FLUKA atmospheric  $\nu$  flux calculation* Proc. of Taup 2001, Sep. 8-12 2001, Assergi (Italy).
  50. J. Ranft, hep-ph/9911213.
  51. G. Fiorentini, V.A. Naumov, & F.L. Villante, Phys. Lett. **B510** (2001) 173 (2001) and Proc. of the 27th Int. Cosmic Ray Conf. **3** (2001) 1218.
  52. T.K. Gaisser and M. Honda, to be published in Annual Review of Nuclear Science.
  53. Y. Tserkovnyak, R.J. Komar, C.W. Nally, & C.E. Waltham Proc. of the 27th Int. Cosmic Ray Conf. **3** (2001) 1196.
  54. J. Wentz et al. Proc. of the 27th Int. Cosmic Ray Conf., **3** (2001) 1167
  55. Y. Liu, L. Derome & M. Buénerd, Proc. of the 27th Int. Cosmic Ray Conf. **3** (2001) 1033.
  56. V. Plyaskin, Phys. Lett. **B516** (2001) 213.
  57. H. Fesefeldt, Aachen preprint PITHA 85/02 (1985).
  58. F. Carminati and I. Gonzales Caballero, ALICE internal note ALICE-INT-2001-041, CERN, (2001). Available at  
[http://edmsoraweb.cern.ch:8001/cedar/doc.info?document\\_id=331045&version=1](http://edmsoraweb.cern.ch:8001/cedar/doc.info?document_id=331045&version=1)
  59. Q.R. Ahmad et al (SNO Collab.), nucl-ex/0204008 and nucl-ex/0204009, submitted to Phys. Rev. Lett.
  60. V. Plyaskin, private communication, May 2002.
  61. This extension is under way as a part of the program of the current development of FLUKA inside INFN.

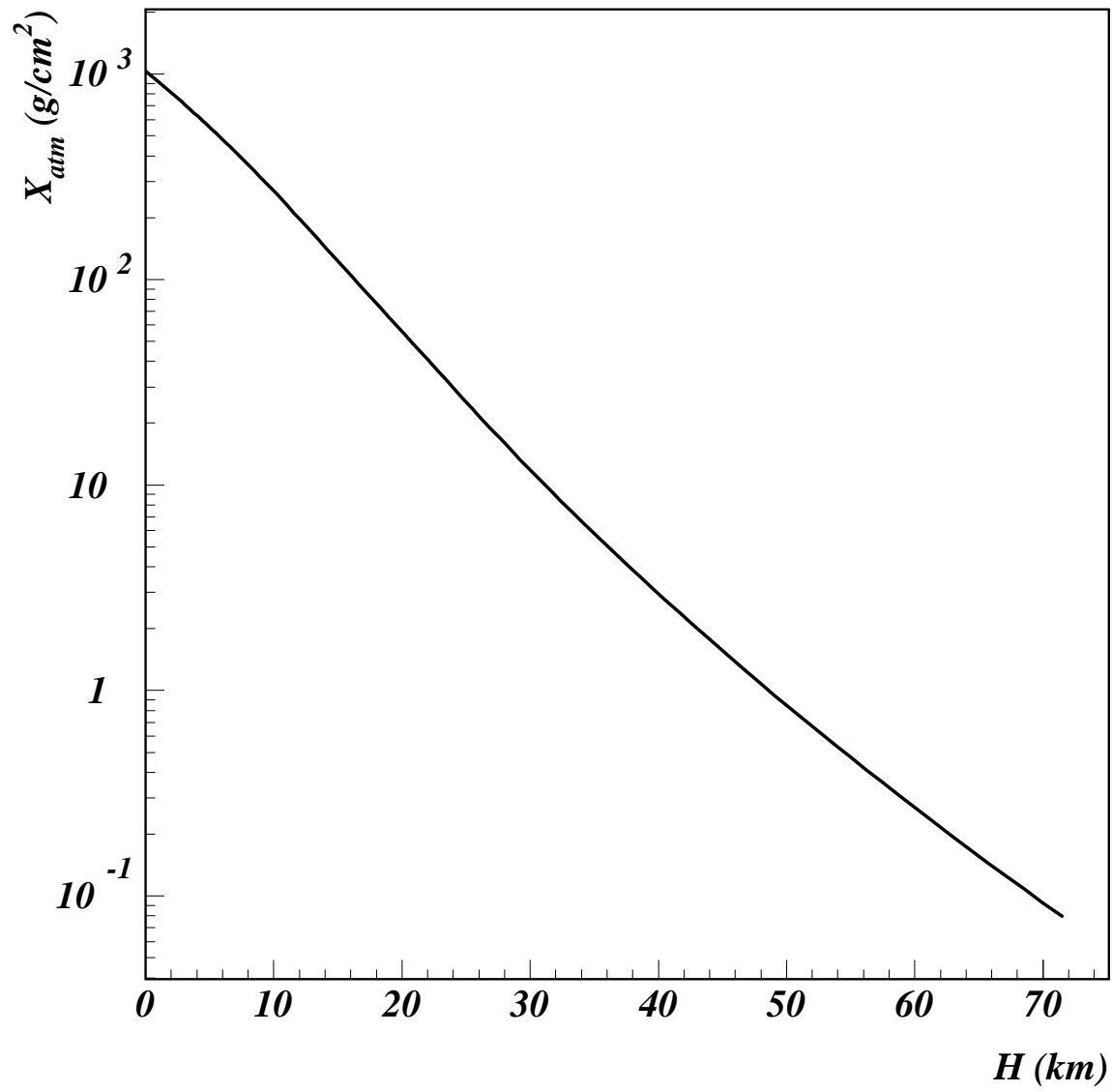


Figure 1. Vertical atmospheric depth as a function of height above sea level as used in the FLUKA simulation.

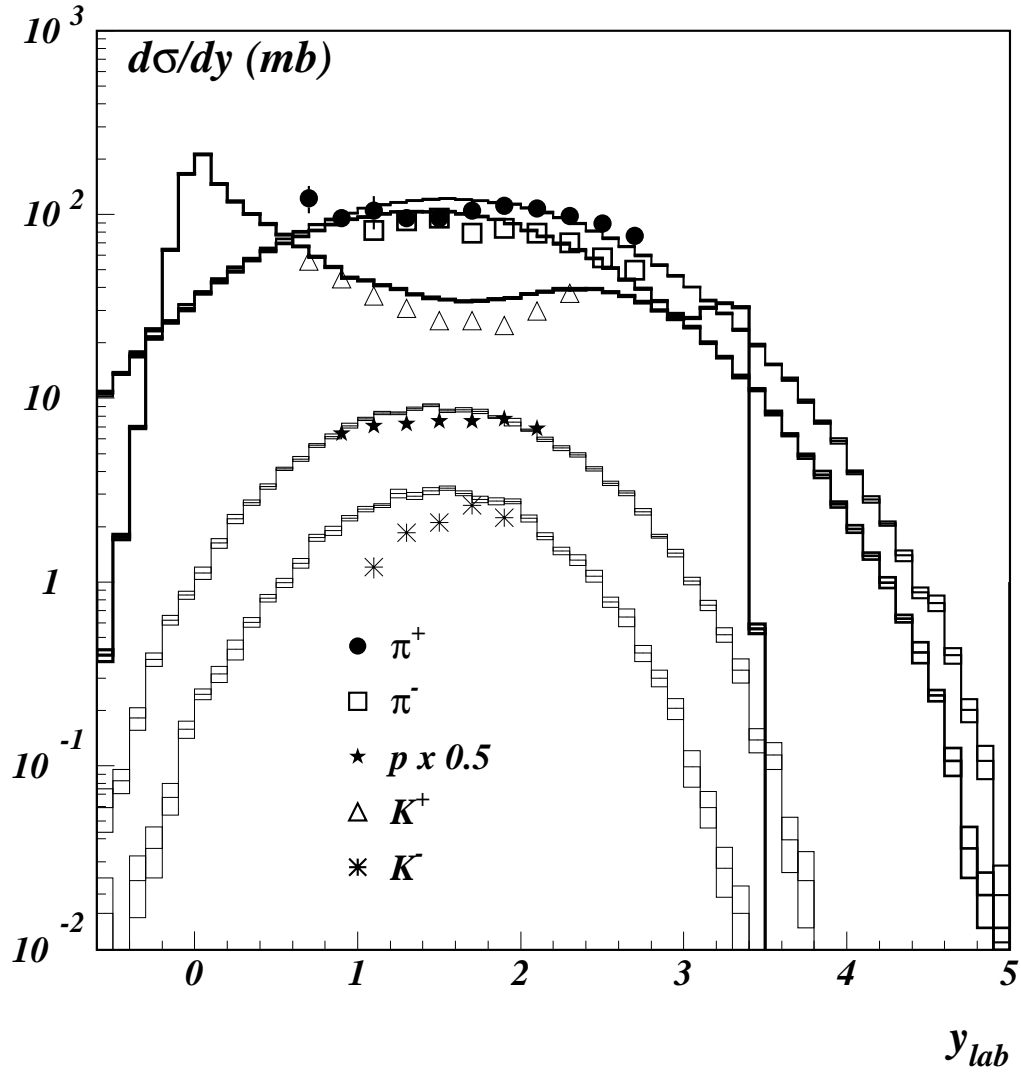


Figure 2. Rapidity distribution of  $\pi^{+/-}$ ,  $K^{+/-}$  and protons for 14.6 GeV/c protons on Be (data from ref. [ 36]). Histograms are simulated data.



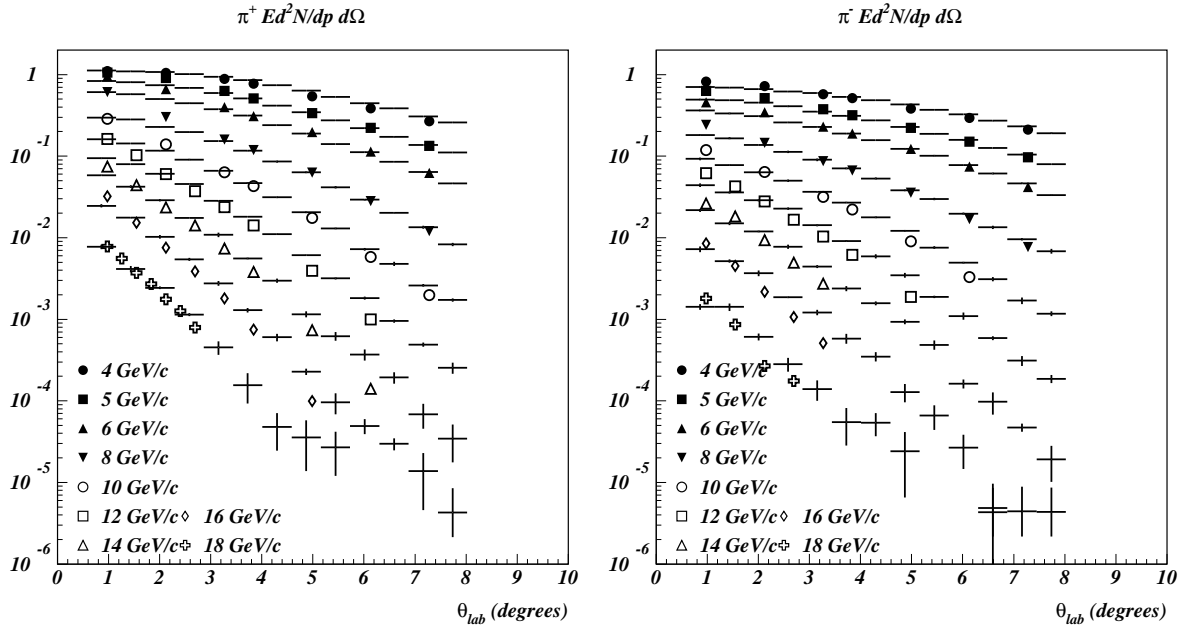


Figure 3. Double differential particle yield for  $\pi^+$  (left) and  $\pi^-$  (right) for 24 GeV/c protons on Be (symbols extrapolated from the double differential cross section reported in ref. [ 37]). Histograms are simulation results. Data are given as a function of  $\theta_{lab}$  for different momentum bins.

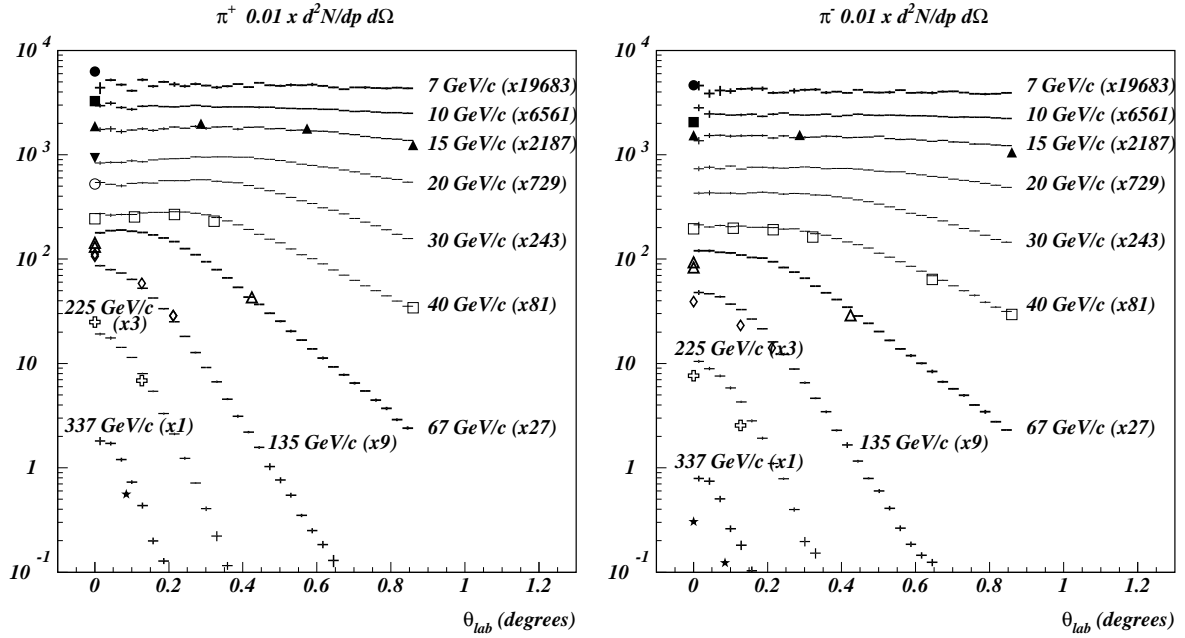


Figure 4. Double differential cross section for  $\pi^+$  (left) and  $\pi^-$  (right) production for 450 GeV/c protons on a 10 cm thick Be target (data from ref. [ 38] and [ 39]). Histograms are simulation results. Data are given as a function of  $\theta_{lab}$  for different momentum bins. The distributions are scaled by increasing factors (reported in the figure) to allow a clearer separation.

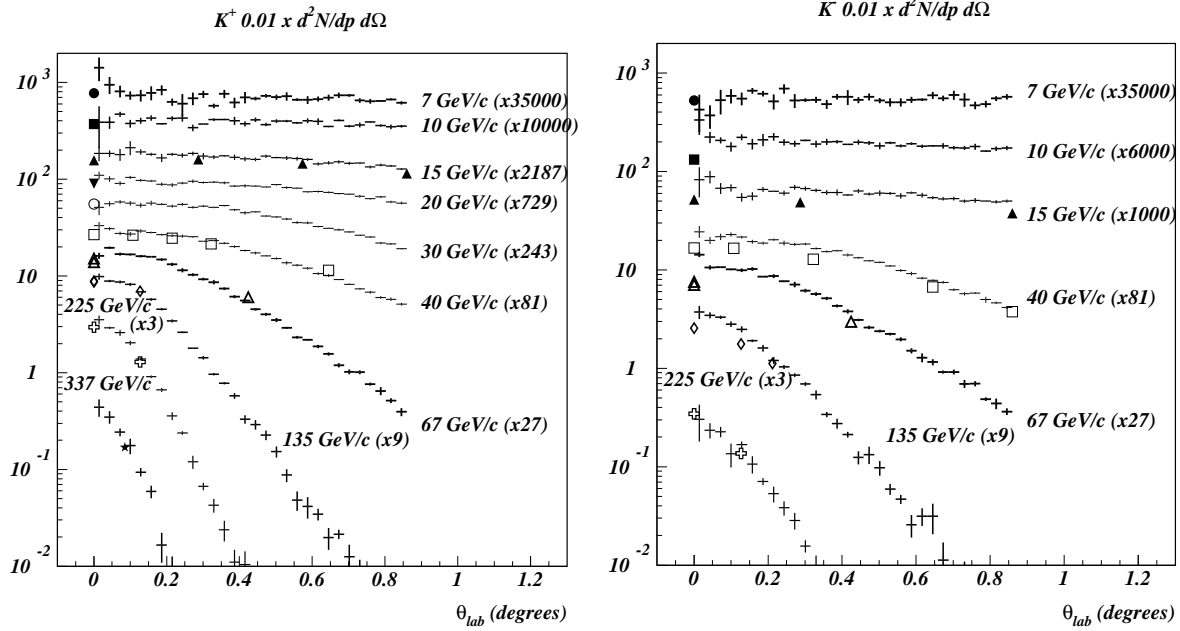


Figure 5. Double differential cross section for  $K^+$  (left) and  $K^-$  (right) production for 450 GeV/c protons on a 10 cm thick Be target (data from ref. [38] and [39]). Histograms are simulation results. Data are given as a function of  $\theta_{lab}$  for different momentum bins. The distributions are scaled by increasing factors (reported in the figure) to allow a clearer separation.

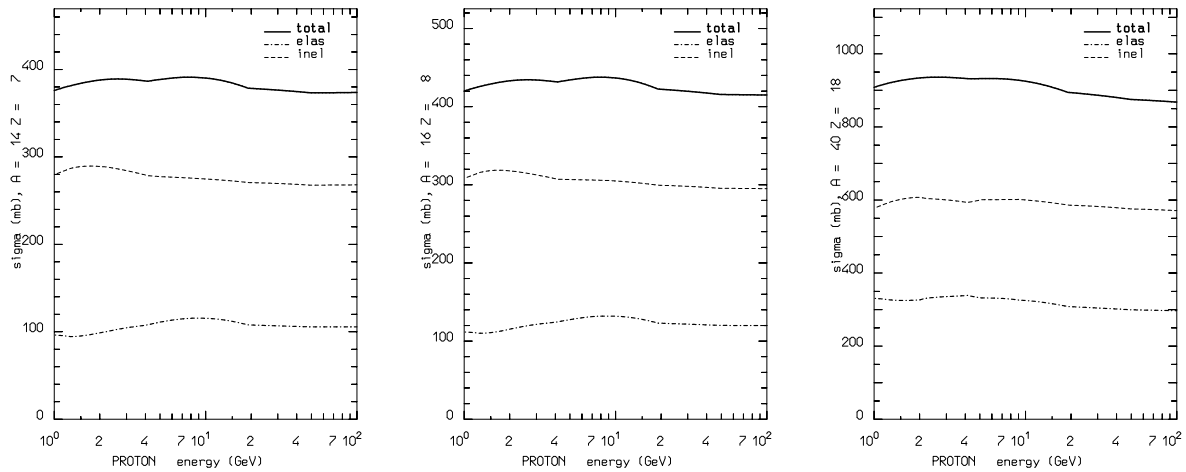


Figure 6. FLUKA cross section as a function of proton kinetic energy for collisions with Nitrogen (left), Oxygen (center) and Argon (right), in the kinetic energy range 1–100 GeV. Top curve is the total cross section, intermediate curve is inelastic cross section while the bottom curve is the elastic one,

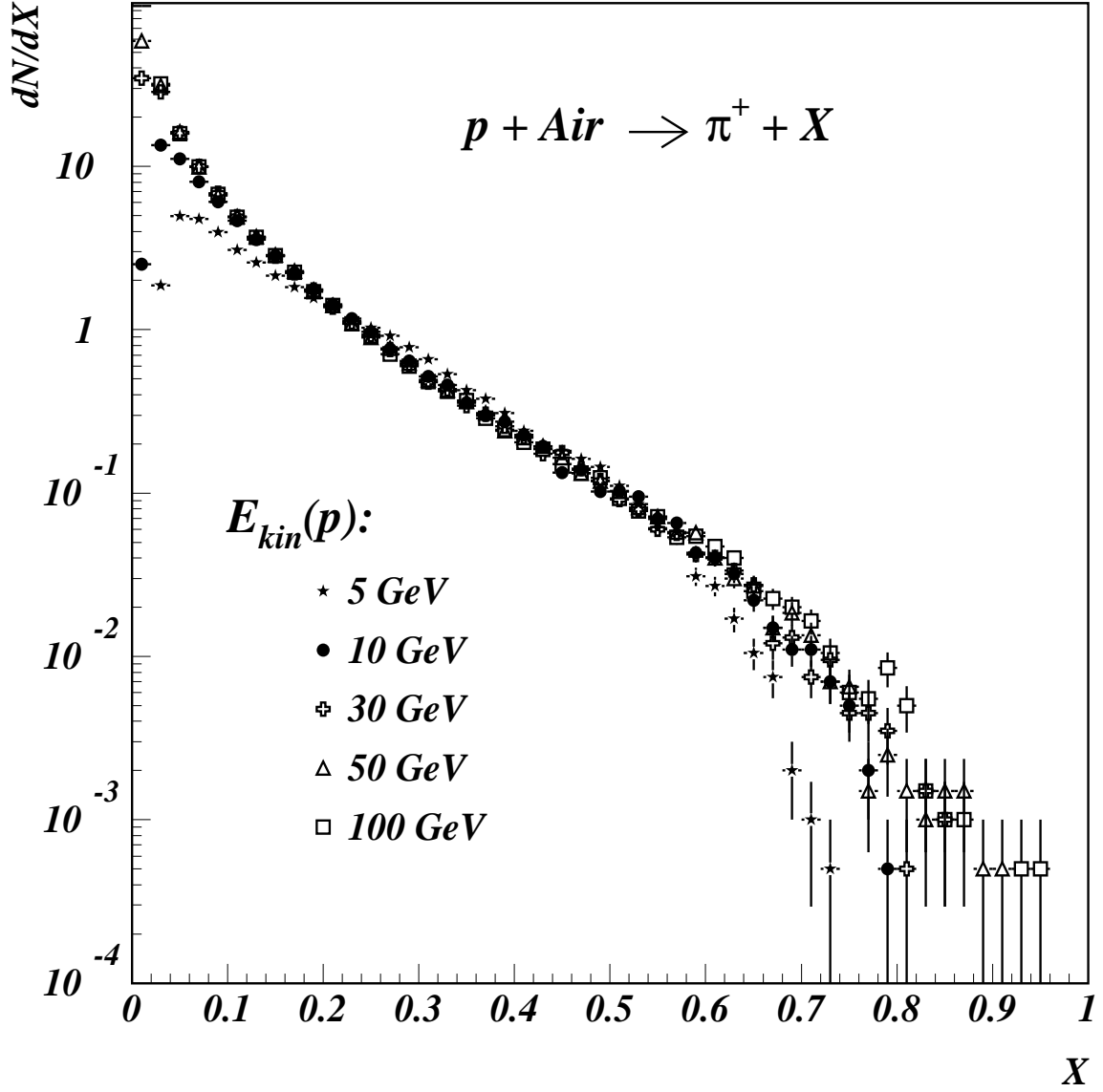


Figure 7.  $dN/dx_{lab}$  for positive pions produced by FLUKA in p–Air collisions at different kinetic energies of the proton projectile.

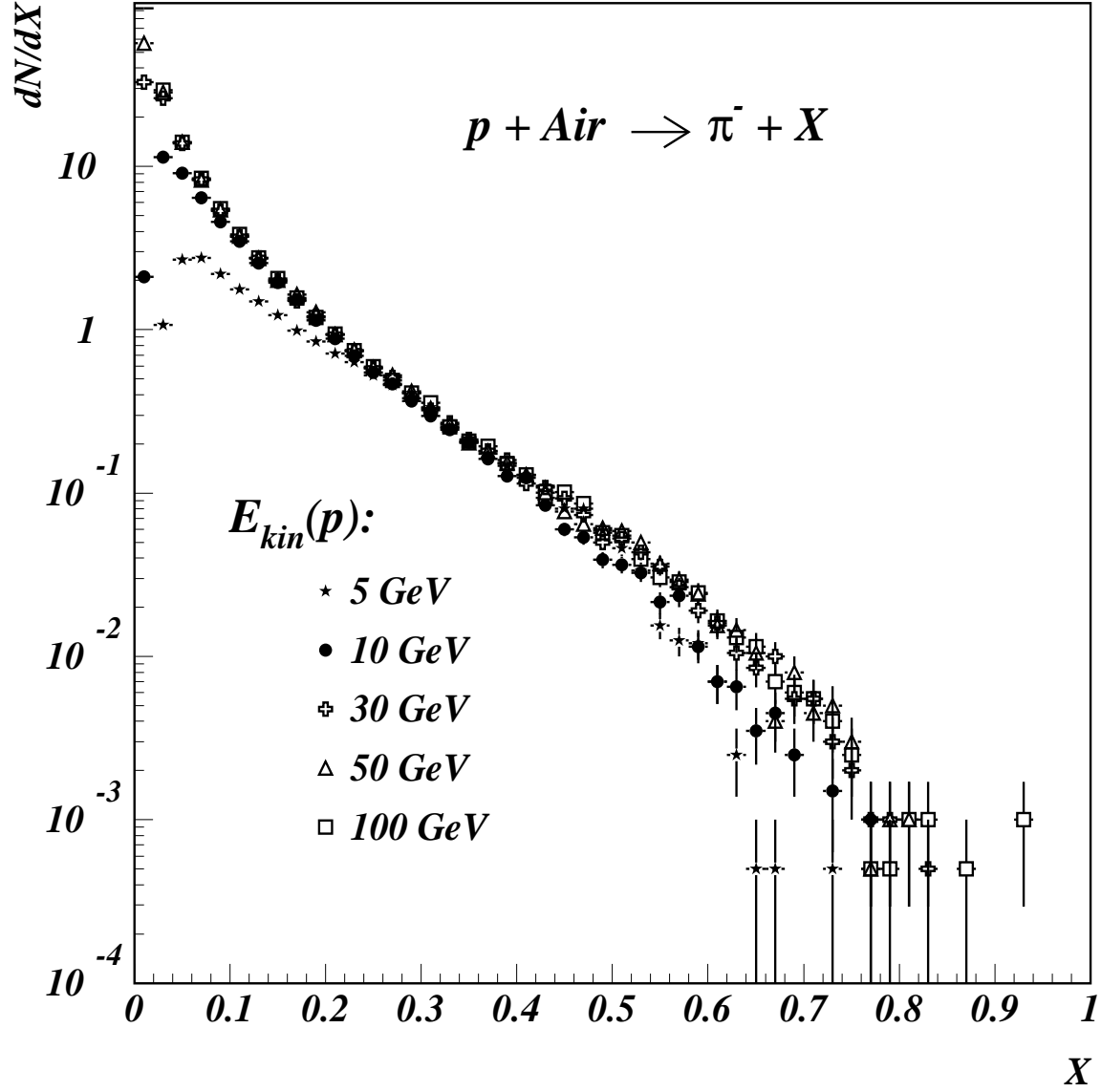


Figure 8.  $dN/dx_{lab}$  for negative pions produced by FLUKA in p–Air collisions at different kinetic energies of the proton projectile.

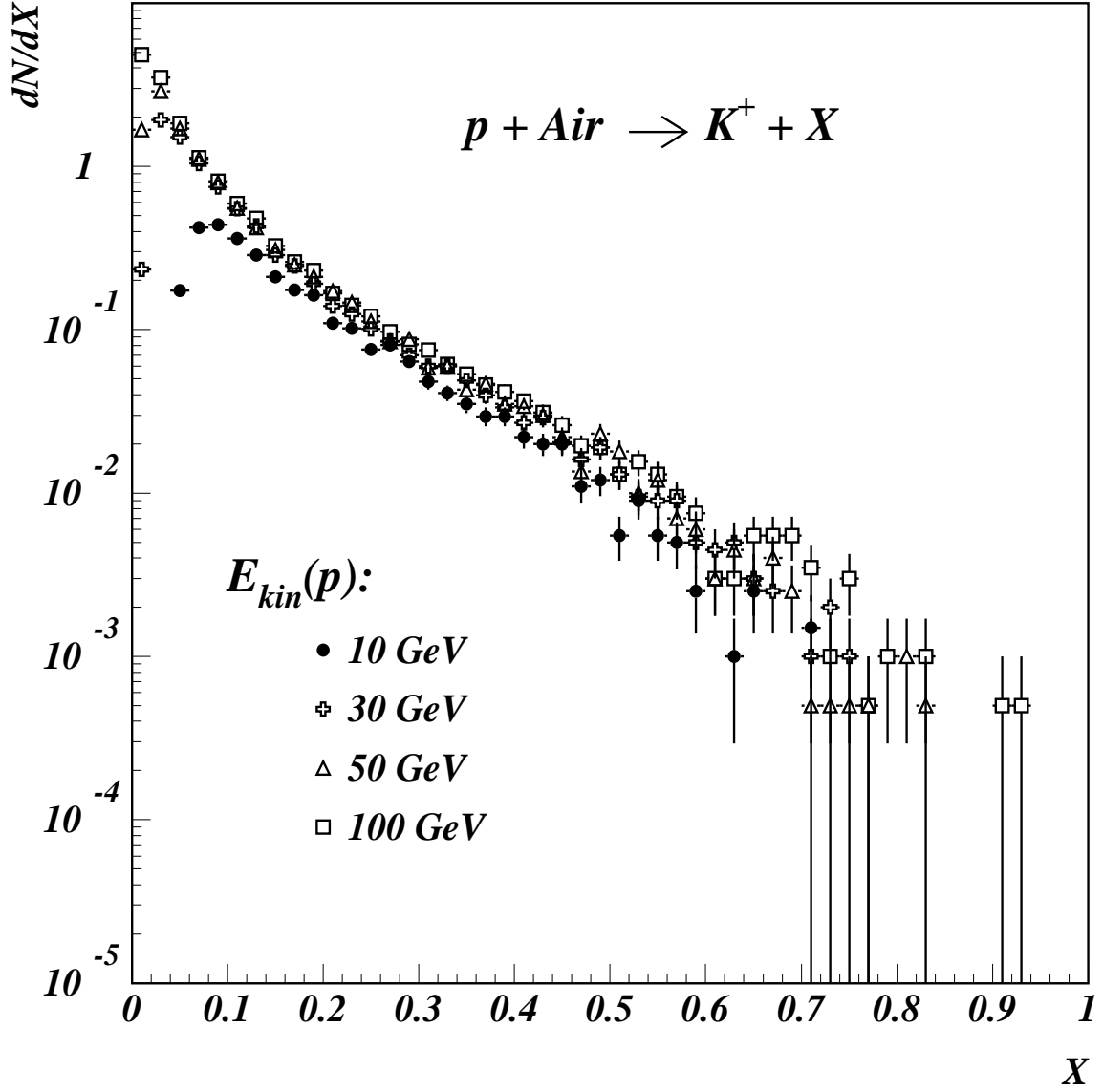


Figure 9.  $dN/dx_{lab}$  for positive Kaons produced by FLUKA in p–Air collisions at different kinetic energies of the proton projectile.

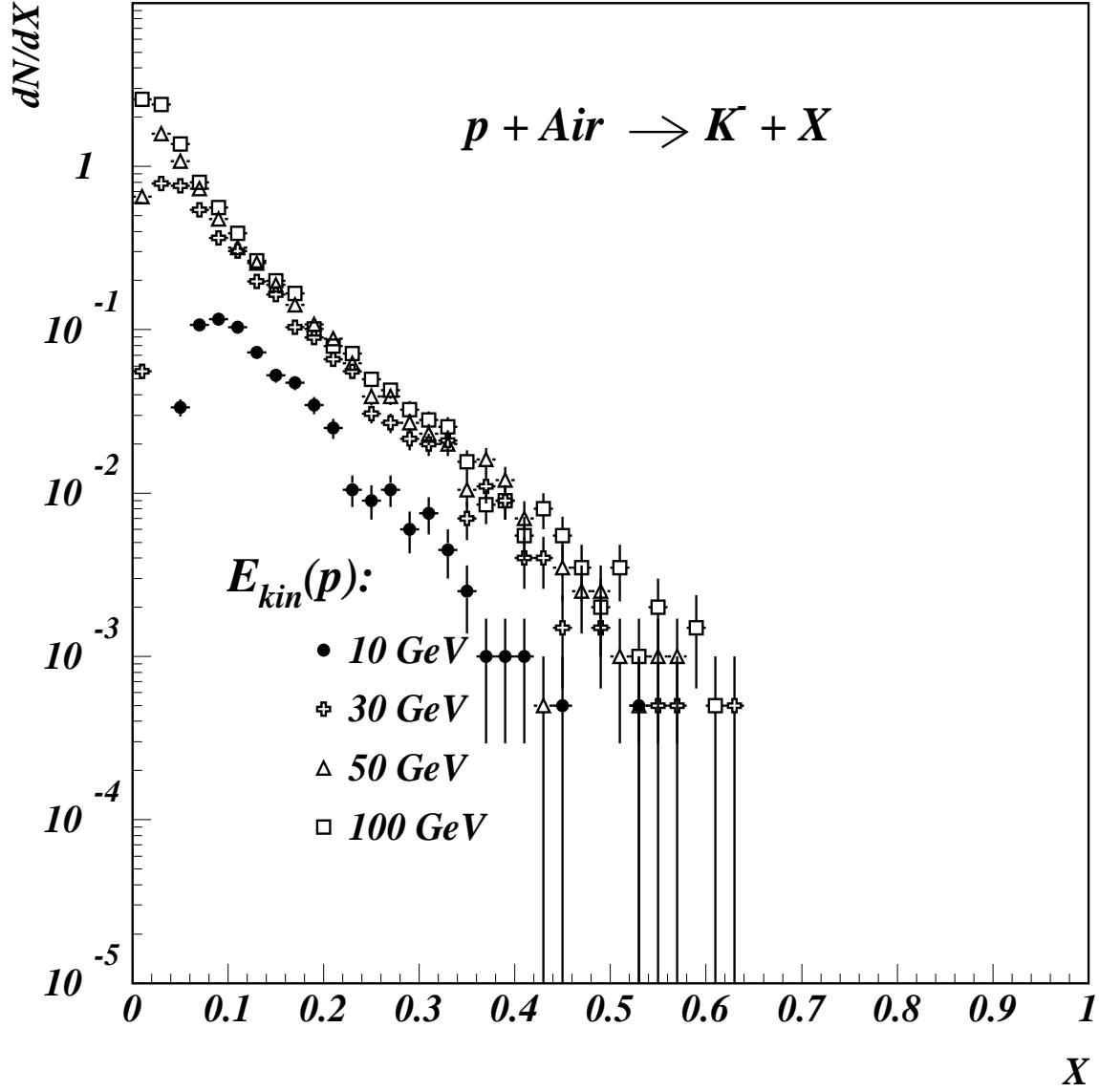


Figure 10.  $dN/dx_{lab}$  for negative Kaons produced by FLUKA in p–Air collisions at different kinetic energies of the proton projectile.

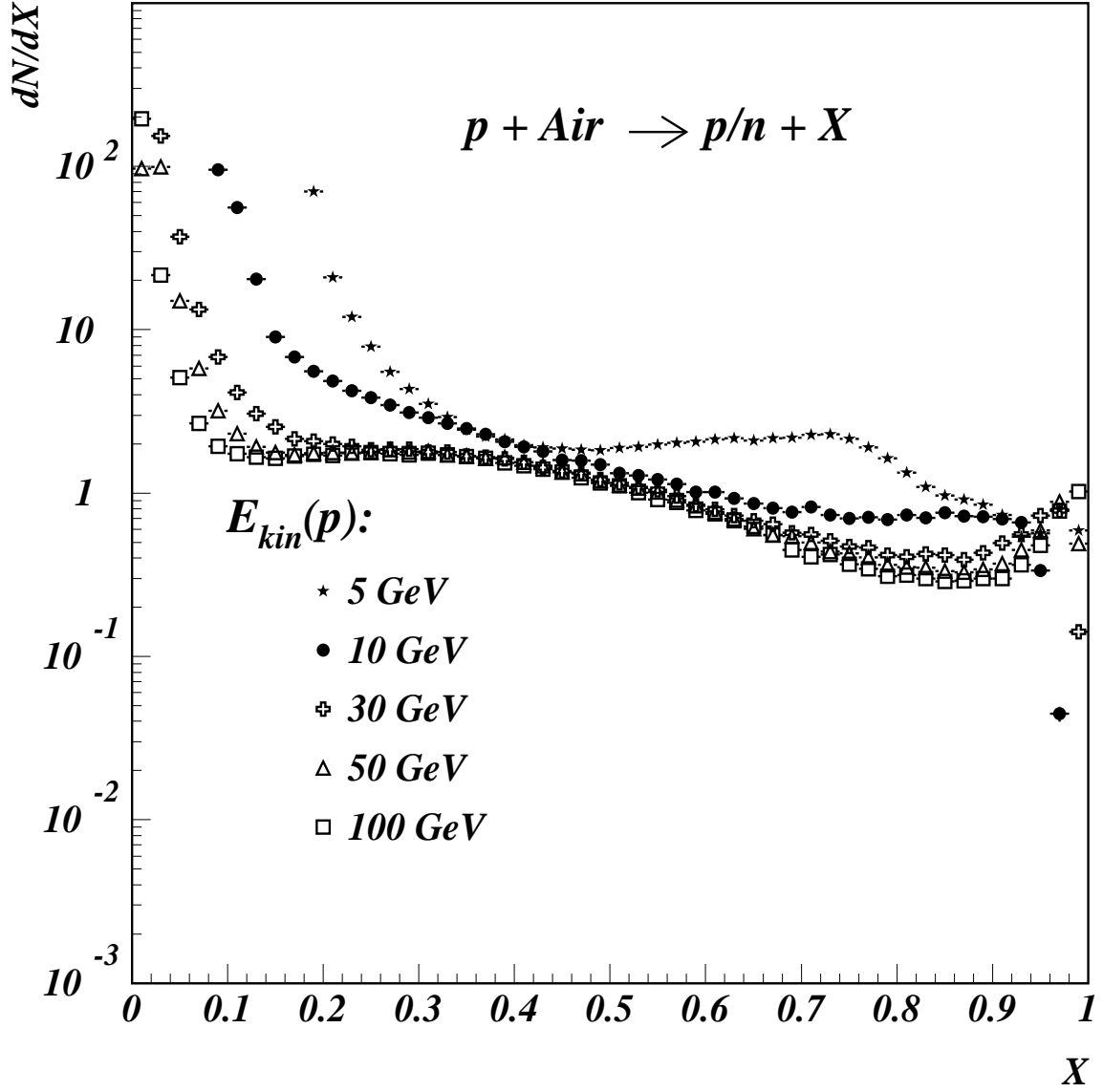


Figure 11.  $dN/dx_{lab}$  for nucleons produced by FLUKA in p–Air collisions at different kinetic energies of the proton projectile.



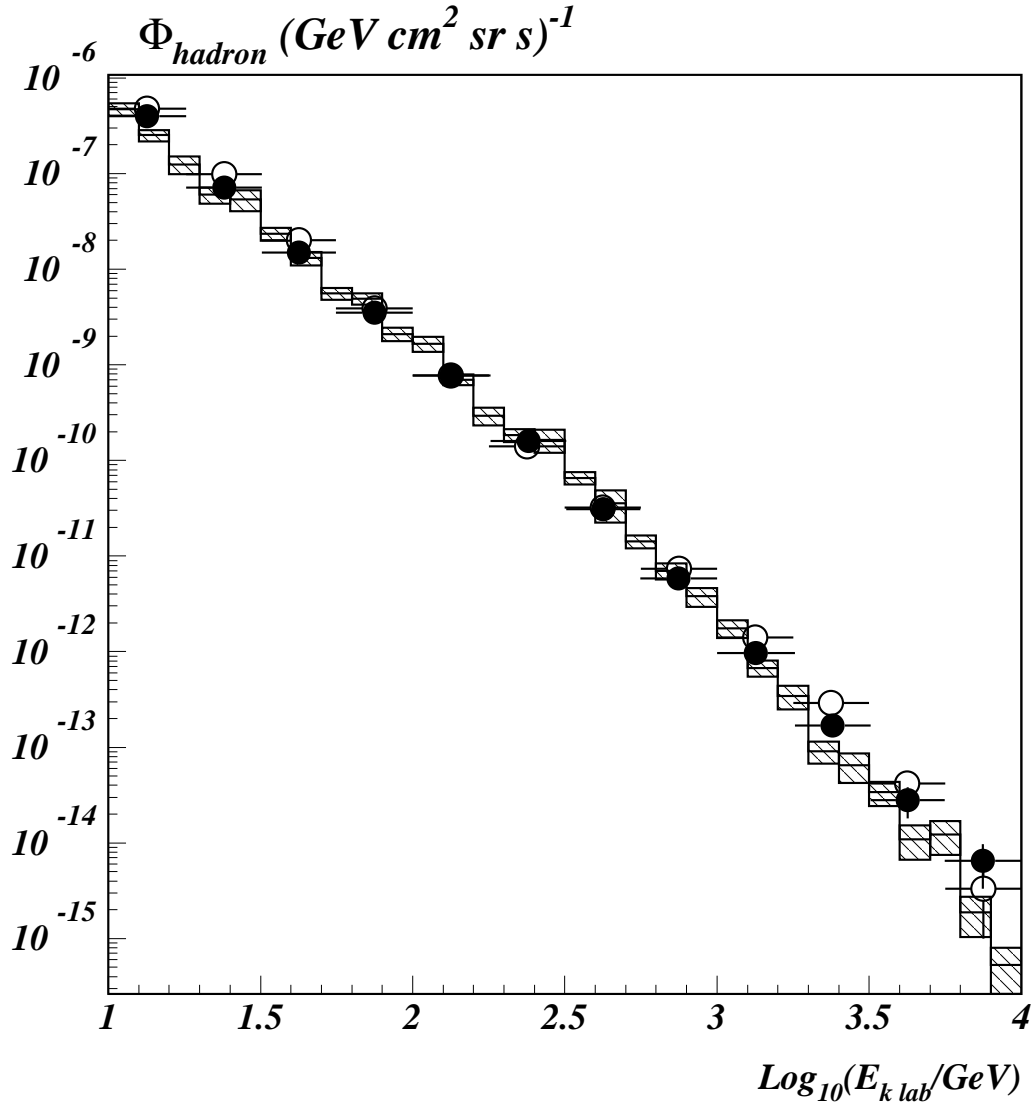


Figure 12. Hadron flux referred to the vertical as measured with the calorimeter of the KASCADE experiment. Histogram is simulation result. Two different sets of experimental data are shown, corresponding to two different angular acceptances, from ref.[ 44] (black symbols: maximum zenith angle 30°) and ref.[ 45] (open symbols: maximum zenith angle 60°).

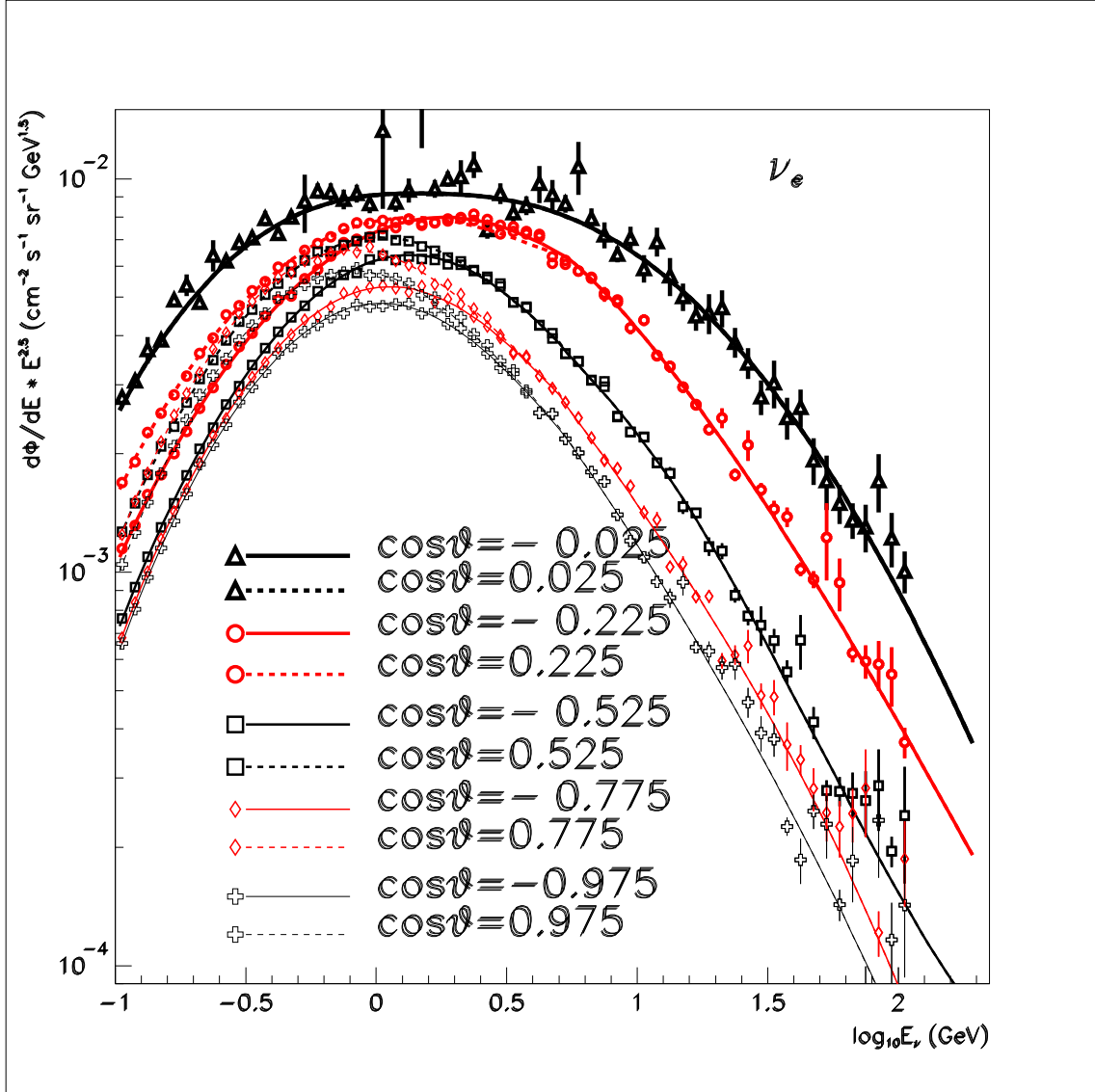


Figure 13. Electron neutrino differential flux times  $E^{2.5}$  versus neutrino energy at Super-Kamiokande site and for solar maximum. The average cosmic ray fit is used. Different curves are for different cosine of the zenith angle values. Lines are the result of the fits of the simulation results described in the text. Solid lines are for the lower hemisphere values, while dashed lines are for upper hemisphere angles. Notice that for the same absolute value of  $\cos\theta$  the solid and dashed lines do not overlap for energies  $\lesssim 5$  GeV while they do overlap at larger energies (where the geomagnetic cut-off does not produce any effect) and at the horizon. Symbols show the simulation results in order to show the agreement with the fits. Notice at very large angles and at large energies simulation errors are noticeable and the fits are useful to smooth simulation points.

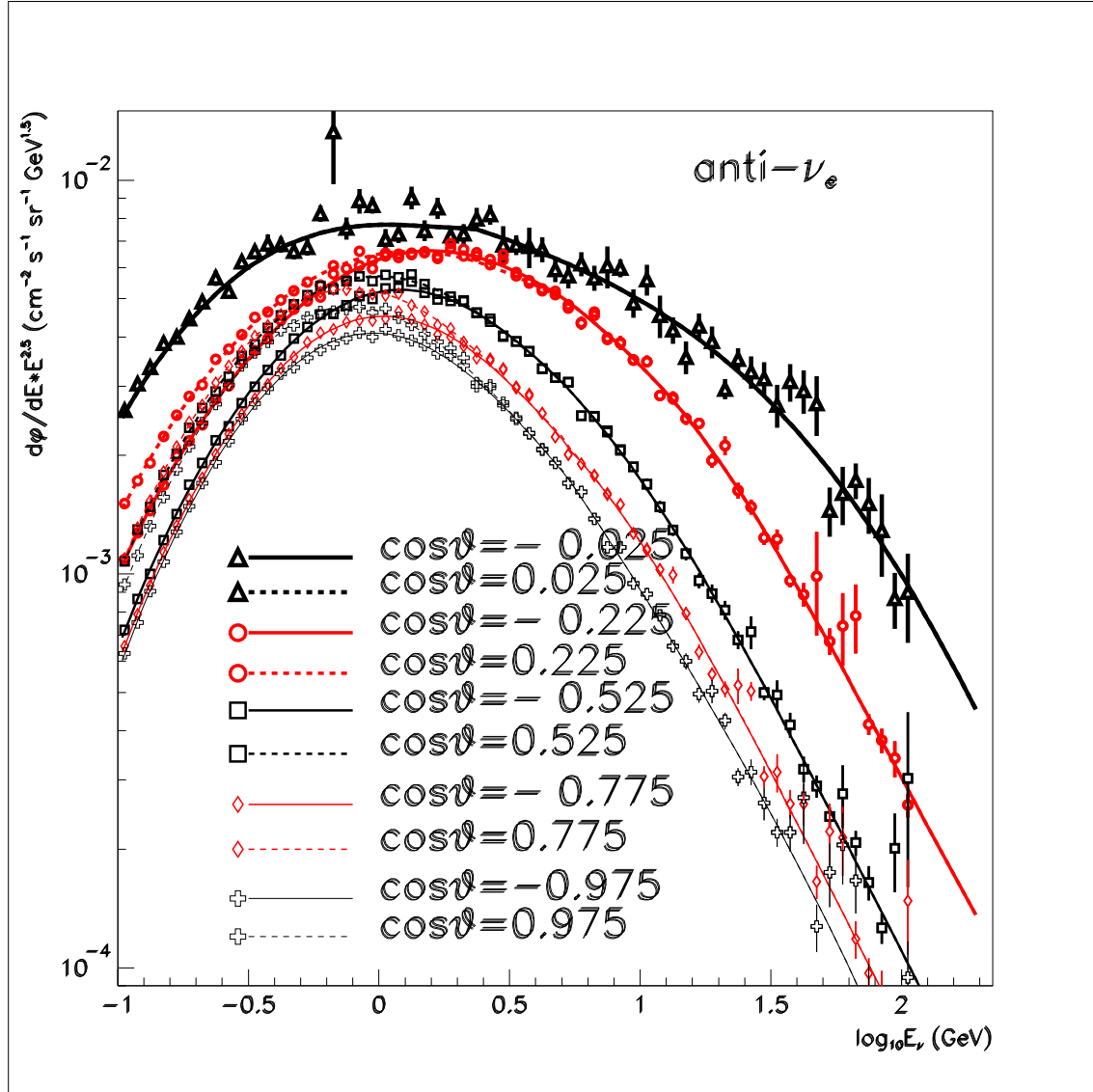


Figure 14. Electron anti-neutrino differential flux times  $E^{2.5}$  versus neutrino energy at Super-Kamiokande site and for solar maximum. More details in the caption of Fig. 13.

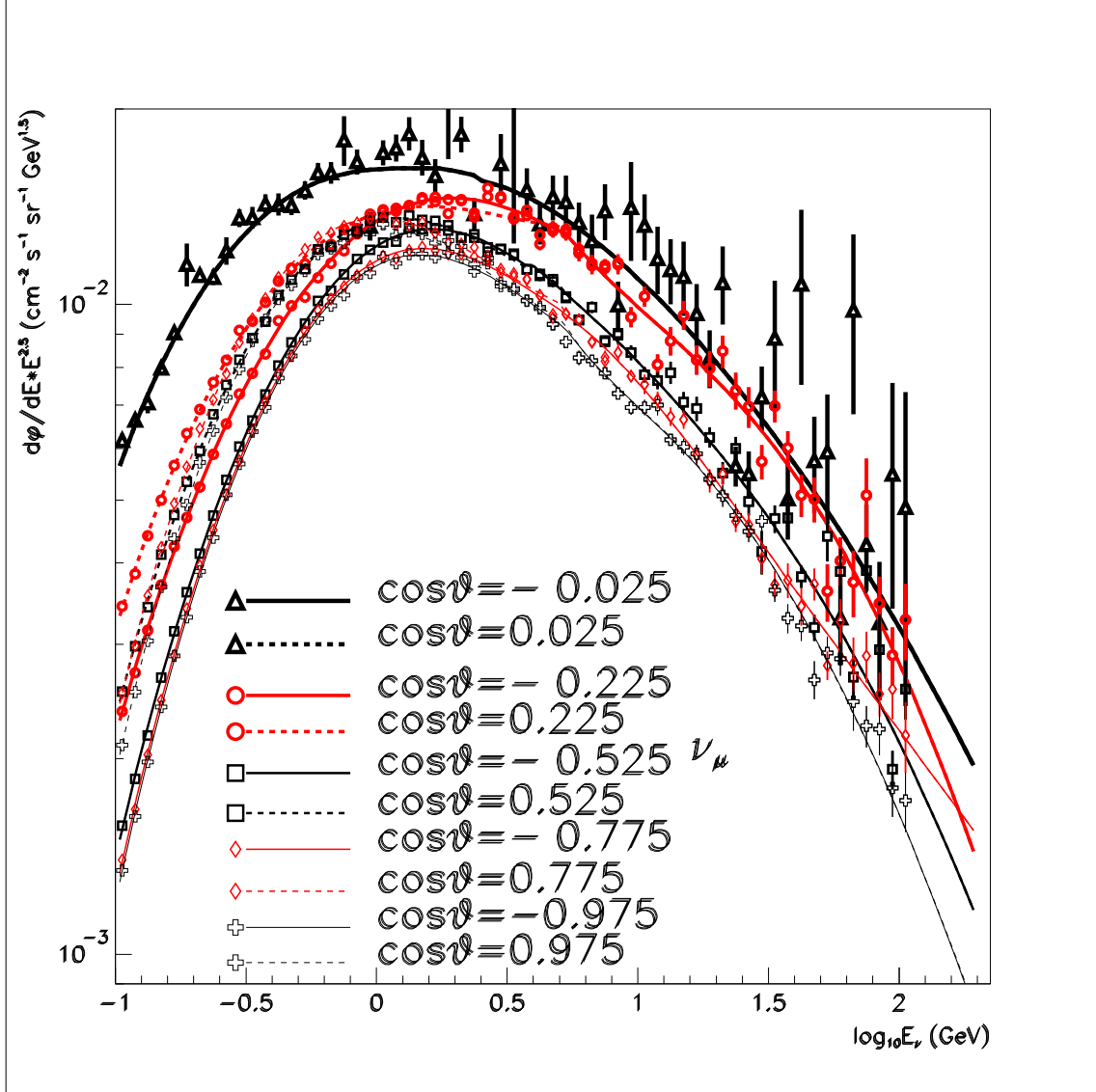


Figure 15. Muon neutrino differential flux times  $E^{2.5}$  versus neutrino energy at Super-Kamiokande site and for solar maximum. More details in the caption of Fig. 13.

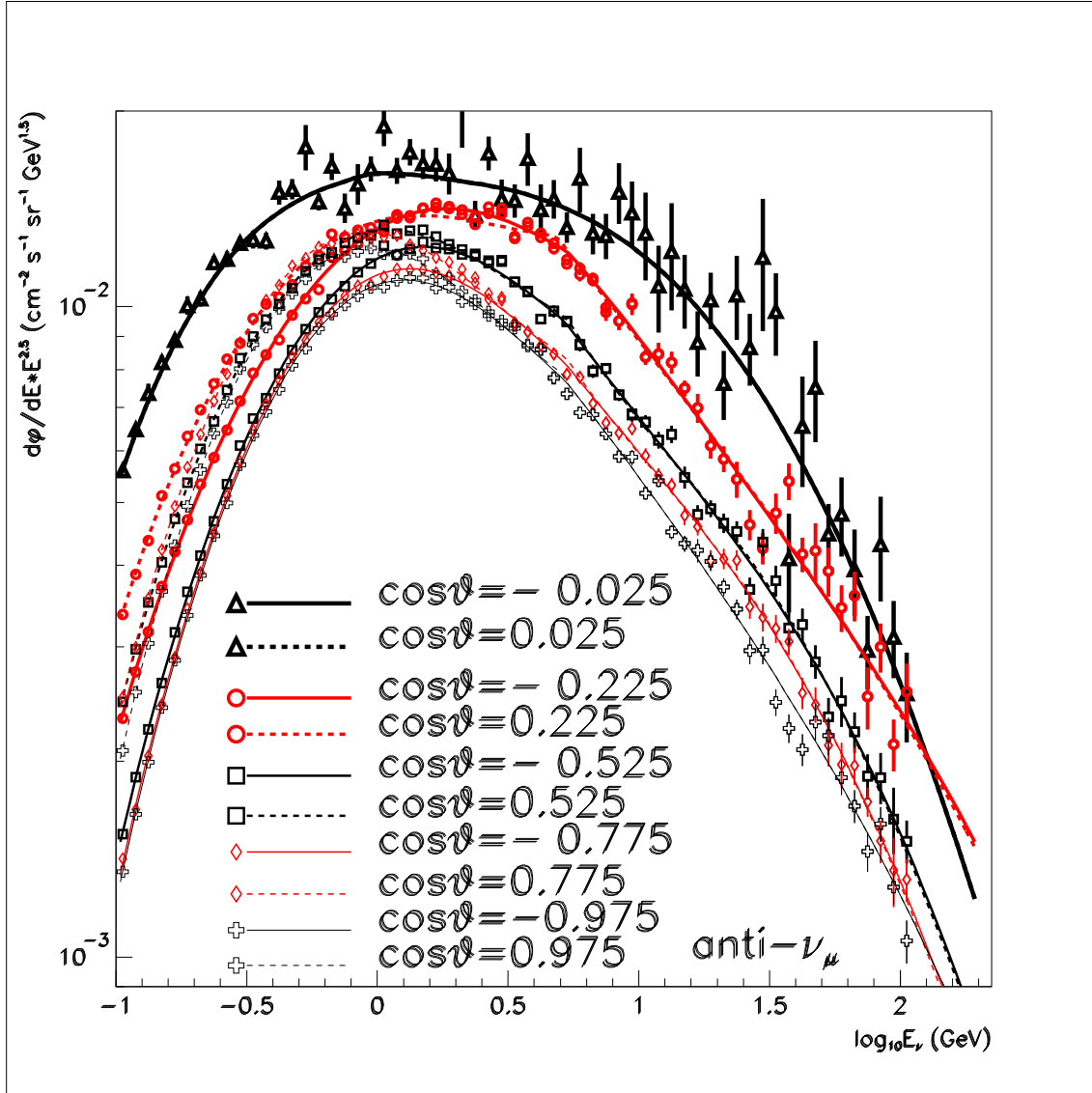


Figure 16. Muon anti-neutrino differential flux times  $E^{2.5}$  versus neutrino energy at Super-Kamiokande site and for solar maximum. More details in the caption of Fig. 13.

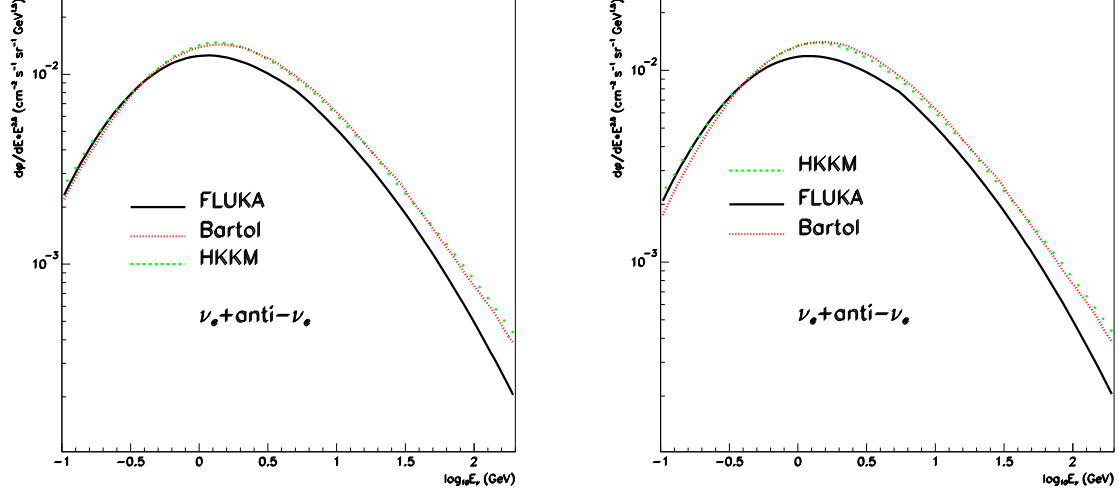


Figure 17. Electron neutrino and anti-neutrino differential flux times  $E^{2.5}$ , angle averaged over the whole solid angle, versus neutrino energy at Super-Kamiokande site for solar minimum (left) and solar maximum (right) for the FLUKA calculation (solid line), the Bartol one (dotted line) [ 11] and for HKKM [ 18] (dashed line).

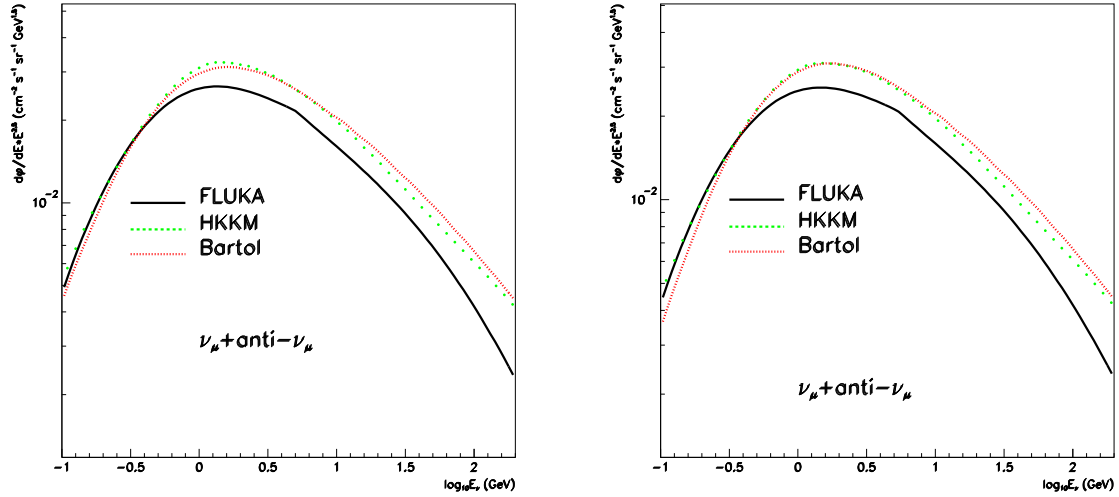


Figure 18. Muon neutrino and anti-neutrino differential flux times  $E^{2.5}$ , angle averaged over the whole solid angle, versus neutrino energy at Super-Kamiokande site for solar minimum (left) and solar maximum (right) for the FLUKA calculation (solid line), the Bartol one (dotted line) [ 11] and for HKKM [ 18] (dashed line).

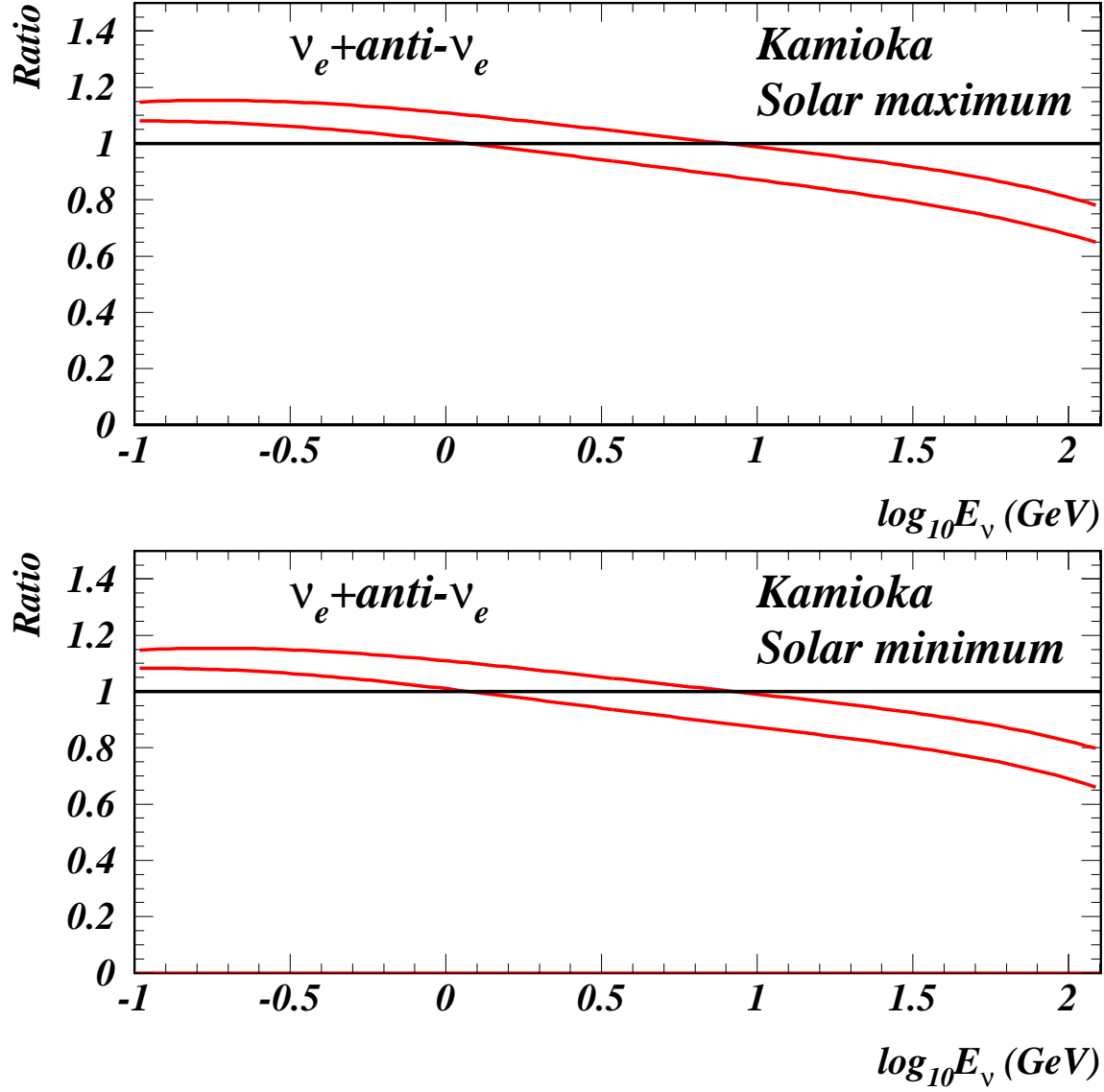


Figure 19. Muon neutrino and anti-neutrino ratio of fluxes averaged over solid angle versus neutrino energy at Super-Kamiokande site and for solar maximum and solar minimum. The ratio is done between the FLUKA calculation using the recent fit to new measurements of primary cosmic rays over the same calculation using the previous primary cosmic ray flux used in Ref.[ 11]. The 2 lines forming a band represent the uncertainty on the new fit of primaries.

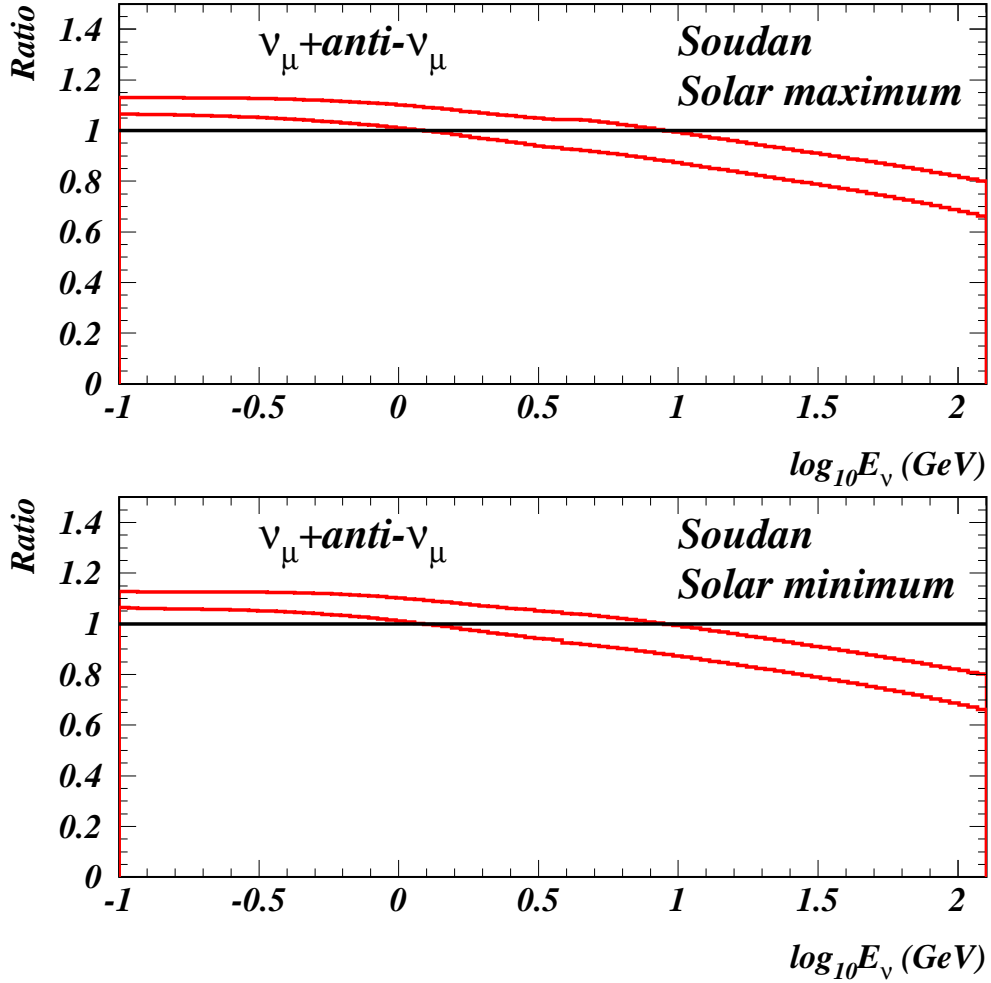


Figure 20. Muon neutrino and anti-neutrino ratio of fluxes averaged over solid angle versus neutrino energy at Soudan site and for solar maximum and solar minimum. The ratio is done between the FLUKA calculation using the recent fit to new measurements of primary cosmic rays over the same calculation using the previous primary cosmic ray flux used in Ref.[ 11]. The 2 lines framing a band represent the uncertainty on the new fit of primaries.